ACCSCIENCE PUBLISHING

Journal of Seismic Exploration

ARTICLE

Critical metal enrichment in coal-bearing strata of the eastern Ordos Basin: A geophysical and geochemical study

Yi Yang[1], Jingtao Zhao[2]*, Suzhen Shi[1], and Wanli Gao[1]

[1]College of Geoscience and Survey Engineering, China University of Mining and Technology (Beijing), Beijing, China

[2]College of Water Sciences, Beijing Normal University, Beijing, China

Abstract

Coal-bearing strata hold significant potential for critical metal resources. This study investigates their enrichment mechanisms in the eastern Ordos Basin using an integrated geophysical-geochemical approach. We combine seismic impedance inversion, tectonic evolution, and log facies interpretation with geochemical data (total organic carbon, sulfur, vitrinite reflectance, trace/rare earth elements) to reconstruct the sedimentary-tectonic-hydrogeological evolution. Results show notable enrichment of zirconium, chromium (Cr), nickel, and hafnium. Seismic facies indicate that deltaic distributary channels and tidal sandbars were primary conduits for metal-bearing fluids. The Taiyuan Formation was deposited in a warm-humid, freshwater-influenced tidal delta-barrier island system under reducing conditions, enabling initial metal sequestration via sulfidation and organic complexation. Reconstruction of tectonic evolution confirms that Yanshanian tectono-thermal events associated with the Zijinshan pluton generated fault networks that channeled hydrothermal fluids, driving secondary metal enrichment. Groundwater circulation, controlled by sedimentary facies and fractures, further regulates metal remobilization. A focused study on Cr delineates a three-stage enrichment model: source weathering, sedimentary reduction, and tectonic-hydrothermal activation. This work establishes a structure–sedimentation–groundwater coupled joint ore-controlling model, underscoring the value of integrated geophysical and geochemical methods for exploring critical metals in coal-bearing strata.

Keywords: Coal measures; Critical metals; Seismic impedance inversion; Enrichment mechanisms; Sedimentary facies; Tectonic-thermal evolution; Groundwater circulation

***Corresponding author:**
Jingtao Zhao
(diffzjt@bnu.edu.cn)

Citation: Yang Y, Zhao J, Shi S, Gao W. Critical metal enrichment in coal-bearing strata of the eastern Ordos Basin: A geophysical and geochemical study. *J Seismic Explor*. 2026;35(2):025520130. doi: 10.36922/JSE025520130

Received: December 24, 2025

Revised: February 10, 2026

Accepted: February 13, 2026

Published online: March 27, 2026

Copyright: © 2026 Author(s). This is an Open-Access article distributed under the terms of the Creative Commons Attribution License, permitting distribution, and reproduction in any medium, provided the original work is properly cited.

Publisher's Note: AccScience Publishing remains neutral with regard to jurisdictional claims in published maps and institutional affiliations.

1. Introduction

Coal-bearing strata are important reservoirs for strategic metals (e.g., gallium [Ga], germanium [Ge], lithium [Li]), offering significant economic potential beyond their conventional use as energy resources.[1,2] In the eastern margin of the Ordos Basin, previous research has primarily focused on coal accumulation and coalbed methane, leaving the enrichment mechanisms of critical metals within the coal measures poorly understood.

Geological structures, such as faults and folds, provide essential pathways and space

for metal-bearing hydrothermal fluids, controlling their migration, focusing, and eventual deposition.[3,4] These tectonic features, including faults, folds, and magmatic bodies, fundamentally influence ore-forming space, permeability, and fluid pathways, thereby governing metal transport and precipitation.[5–7] Multi-source hydrothermal fluids (magmatic, alkaline, volcanic) can mobilize and precipitate metals such as gold (Au) and Ge through interaction with sulfides and carbonates. Volcanic fluids, characterized by low pH, high volatile content, and significant ore-forming elements, act as efficient agents for leaching metals from wall rocks and precipitating them as sulfides or oxides upon cooling or mixing with groundwater.[8] Tectono-magmatic activities regulate both the source and intensity of mineralization[9], with magmatic intrusions enhancing basement leaching[10] and introducing exogenous metals via volcanic ash.[11] Fracture networks serve as primary conduits, controlling both primary enrichment and subsequent reactivation of metals.[12] Regional tectonic evolution exerts long-term control on metallogenesis. For instance, the Caledonian uplift provided structural conditions for Ga enrichment, while Yanshanian tectono-thermal events drove secondary metal enrichment through thermal alteration.[13] Techniques such as layer flattening, balanced sections, and thickness recovery have demonstrated how paleo-tectonic patterns regulate sediment supply and diagenetic fluid flow, ultimately shaping the three-dimensional (3D) distribution of metals in coal measures.[14–16]

Sedimentary environments also play a critical role, with redox conditions, provenance, and lithology collectively governing initial metal concentration and subsequent transformation.[17] In the northern Ordos Basin, the Carboniferous–Permian marine–terrestrial transitional setting established strongly reducing conditions that promoted organic matter adsorption and volcanic ash incorporation, leading to rare earth element (REE) enrichment—evident from characteristic negative europium (Eu) and cerium (Ce) anomalies in coals.[18] Conversely, Jurassic terrestrial oxidation inhibited element preservation. Sedimentary environments further influence syndepositional precipitation and lithofacies control on epigenetic uranium (U) mineralization.[19,20] In the Taiyuan Formation, alternating warm-humid and dry-hot phases favored freshwater anoxic conditions conducive to Ga enrichment. Advances in seismic stratigraphy and stratigraphic slicing now enable quantitative reconstruction of deltaic systems, clarifying how sandbody architecture and microfacies control metal migration.[21–24]

In contrast, the role of groundwater in trace metal enrichment remains understudied.[25–27] Metals such as Ga, selenium, strontium (Sr), zirconium (Zr), REEs, mercury, lead (Pb), and thorium (Th) are often mobilized and enriched through dissolution-reprecipitation during diagenesis and redox interface fluctuations.[28] For example, groundwater leaching has been proposed as a key factor in REE enrichment in Late Permian coal seams in the Sichuan Basin.[29]

In the study area, thick, cyclic coal measures with diverse source-reservoir-cap assemblages present a complex setting.[30–34] While seismic inversion and lithofacies modeling have begun to clarify tectono-sedimentary controls on 3D metal zoning, a comprehensive understanding of the synergistic effects of tectonic, sedimentary, and fluid systems—particularly in the eastern Ordos Basin—is still lacking. Moreover, the contribution of groundwater circulation to metal transport has not been adequately addressed. This study introduces an integrated framework that synergistically combines high-resolution seismic interpretation, geochemical provenance analysis, and paleogroundwater modeling to elucidate the multi-stage enrichment mechanisms of critical metals. Our approach advances the field by: (i) Integrating seismic facies analysis with trace element geochemistry to constrain the sedimentary environment's control on initial metal enrichment; (ii) Reconstructing the Late Paleozoic–Mesozoic tectonic uplift history to clarify the influence of tectono-magmatic activity on metal migration and re-concentration; and (iii) Establishing a structure–sedimentation–groundwater joint control model to provide a predictive framework for metal enrichment in analogous basin settings.

2. Geological setting

The study area is located within the Jinxi flexural fold belt on the eastern margin of the Ordos Basin (Figure 1). The structural pattern is characterized by a north–south orientation as the dominant feature, with faults present in the Paleozoic, yet their scale is limited.[35] In the southern section, there is an evident tectonic and magmatic superposition, and the faults display a semi-circular radial pattern associated with the Zijinshan pluton. Conversely, the northern region remains a slightly deformed area, unaffected by magmatism. The stratigraphic sequence comprises the Carboniferous Benxi Formation, the Taiyuan Formation, the Permian Shanxi Formation, the Lower Shihezi Formation, the Upper Shihezi Formation, and the Shiqianfeng Formation. The primary coal-bearing strata are the Taiyuan Formation and the Shanxi Formation.

3. Materials and methods

The LX-5 well, which is strategically situated in the

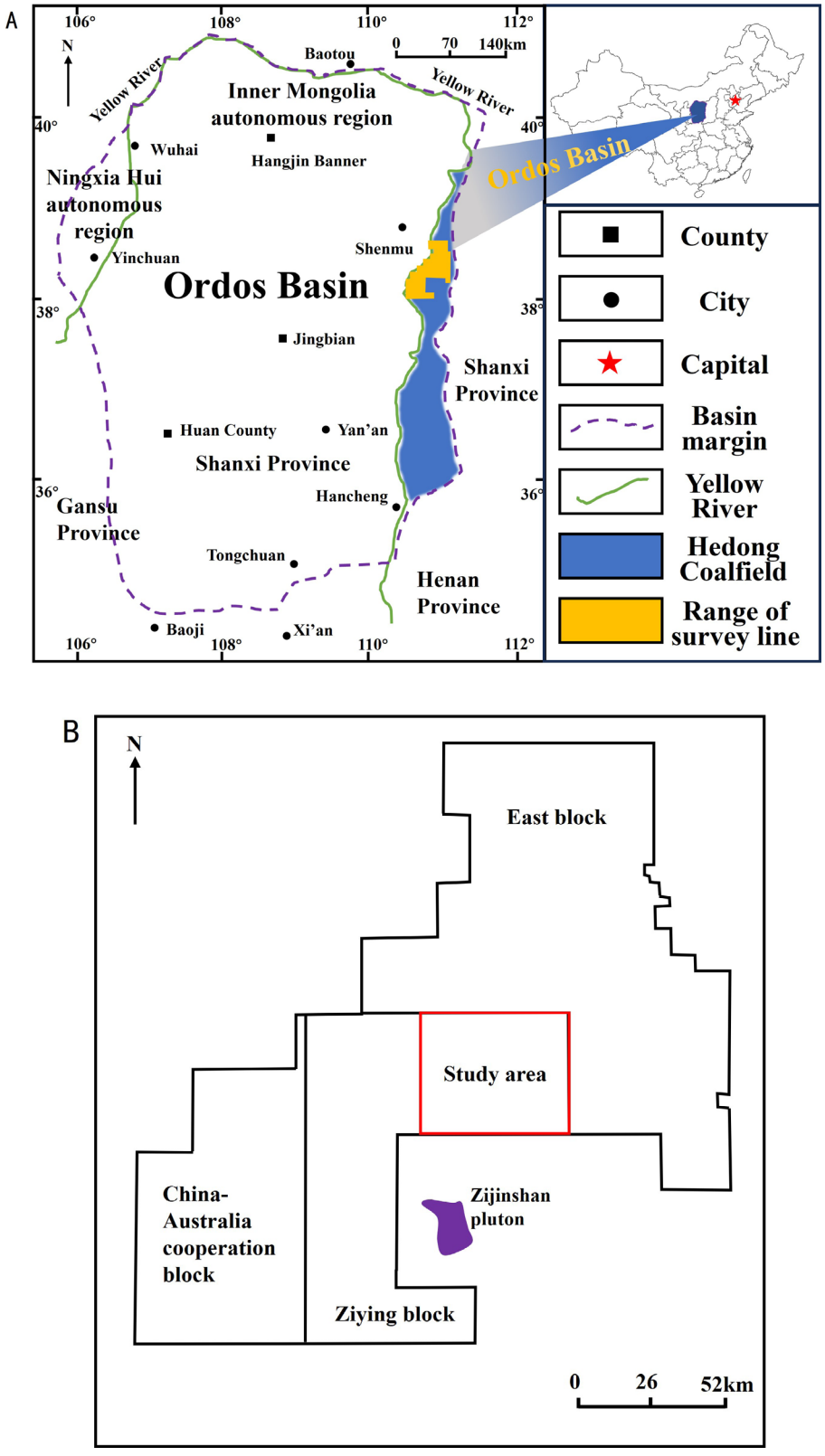


Figure 1. Location of the study area. (A) Geographical location of the Ordos Basin. (B) Distribution of the study area.

southwestern region of the study area (Figure 1B), penetrated the complete and continuous Carboniferous–Permian coal-bearing stratigraphic sequence. To ensure data representativeness and capture the geological variations related to the major depositional and tectonic stages, a systematic, high-density sampling methodology was employed along the entire cored section. Fifty-five core samples were collected at precise depths, encompassing all the major formations (Benxi, Taiyuan, Shanxi, Lower Shihezi, Upper Shihezi, and Shiqianfeng) and their predominant lithologies (coal, mudstone, and sandstone) (Table 1). Subsequently, a comprehensive series of analyses was conducted on this representative sample collection, including total organic carbon (TOC), sulfur (S) content, vitrinite reflectance, major and trace elements, and clay minerals. This stratified and systematic approach ensured that the resulting high-resolution vertical dataset effectively captures the key temporal sequences of processes necessary to investigate the mechanisms governing critical metal enrichment.

All experiments were conducted in the Laboratory of Mineralization and Dynamics at Chang'an University. The analysis and determination of TOC and S content were conducted using the carbon-S analyzer (CS-230, LECO Corporation, USA). Vitrinite reflectance was measured using a microphotometer (MPV-SP, Leica, Germany). Trace elements and REE were analyzed using an inductively coupled plasma mass spectrometer (X-series, Thermo Fisher, USA). Quantitative analysis of the mineral composition was conducted using an X-ray diffractometer (D/max-2200 2035C 4, Rigaku Corporation, Japan).

4. Results and discussion

4.1. Geochemical experiment

4.1.1. Total organic carbon, sulfur content, and vitrinite reflectance

To assess organic matter richness and paleoenvironmental conditions, we measured TOC and S content. Elevated S concentrations often signify anoxic depositional settings, facilitating organic preservation and sulfide formation. Analyses revealed considerable heterogeneity in organic abundance across the sequence. For instance, the Benxi Formation yielded high TOC values (avg. 27.72%), whereas the Upper Shihezi Formation was markedly lean (avg. 0.09%) (Table 1).

4.1.2. Trace, rare earth elements, and mineral composition analysis

The concentrations of trace elements and REE serve as the foundation for a comprehensive exploration of sediment provenance, sedimentation, and diagenesis, as well as for assessing the sedimentary environment. Figure 2 demonstrates that the contents of elements such as Sr, barium (Ba), chromium (Cr), and Pb exhibit significant fluctuations across different formations. The elements with the highest average content are Zr (216.46 μg/g), Ba (164.14 μg/g), and Sr (127.38 μg/g). In the study area, we analyzed the distribution of element content in Carboniferous–Permian strata. Figure 2A illustrates the content distribution of trace elements, where the contents of Ba and Sr are relatively high in the Carboniferous strata, which might be associated with the redox conditions of the sedimentary environment. Figure 2B depicts the REE distribution, showing distinct enrichment characteristics that may reflect changes in sediment provenance and the sedimentary environment.

To gain a comprehensive understanding of the mineral composition of the Upper Shihezi Formation and Benxi Formation, a mineralogical analysis was conducted. Figure 3A depicts the overall mineral composition of the sample, where quartz and clay minerals constitute the primary mineral components. Figure 3B illustrates the relative distribution of clay minerals. Illite and kaolinite are the predominant clay minerals, which implies a sedimentary environment ranging from semi-arid to humid.

4.2. Depositional environment

4.2.1. Sedimentary facies control

The sedimentary facies structure of coal-bearing strata was systematically studied by combining single well facies, cross-section sedimentary facies and seismic constrained plane facies. By establishing a quantitative relationship between well-derived microfacies and optimized seismic attributes (especially RMS amplitude, sweetness, and instantaneous phase), a comprehensive sedimentary model was constructed to reveal a unique delta and barrier island sedimentary system with logging characteristics, sand body geometry, and spatial phase distribution.

(i) Single well facies analysis: The integration of well-log motifs and core lithology from LX-5 facilitated the identification of a deltaic depositional system within the Shanxi Formation. Characteristic features included bell-shaped gamma-ray responses in the mudstones and coals of interdistributary bays, as well as box-shaped profiles associated with distributary channel sandstones. Sedimentary microfacies displayed distinctive log responses. Bell-shaped curves were manifested in the sequences of dark mudstone and coal within interdistributary bays. Deposits of distributary channels, which consisted of fine sandstone, medium sandstone, and pebbly sandstone, generate box-shaped and bell-shaped

Table 1. Geochemical experimental analysis of the Shihezi Formation and Benxi Formation in LX-5 well

Samples	Depth (m)	Formation	Lithology	TOC (weight %)	S (weight %)	Vitrinite reflectance (R0, %)
L5-1-1	1,285.58	Upper Shihezi	Mudstone	0.09	0.01	1.09
L5-1-3	1,619.57	Lower Shihezi	Mudstone	0.65	0.01	0.96
L5-1-7	1,735.41	Taiyuan	Mudstone	7.69	0.90	0.92
L5-1-8	1,736.58	Taiyuan	Carbonaceous mudstone	7.29	0.31	0.94
L5-1-12	1,784.74	Benxi	Mudstone	1.13	0.56	1.65
L5-1-11	1,784.74	Benxi	Coal	54.32	0.43	0.98

Abbreviations: S: Sulfur; TOC: Total organic carbon.

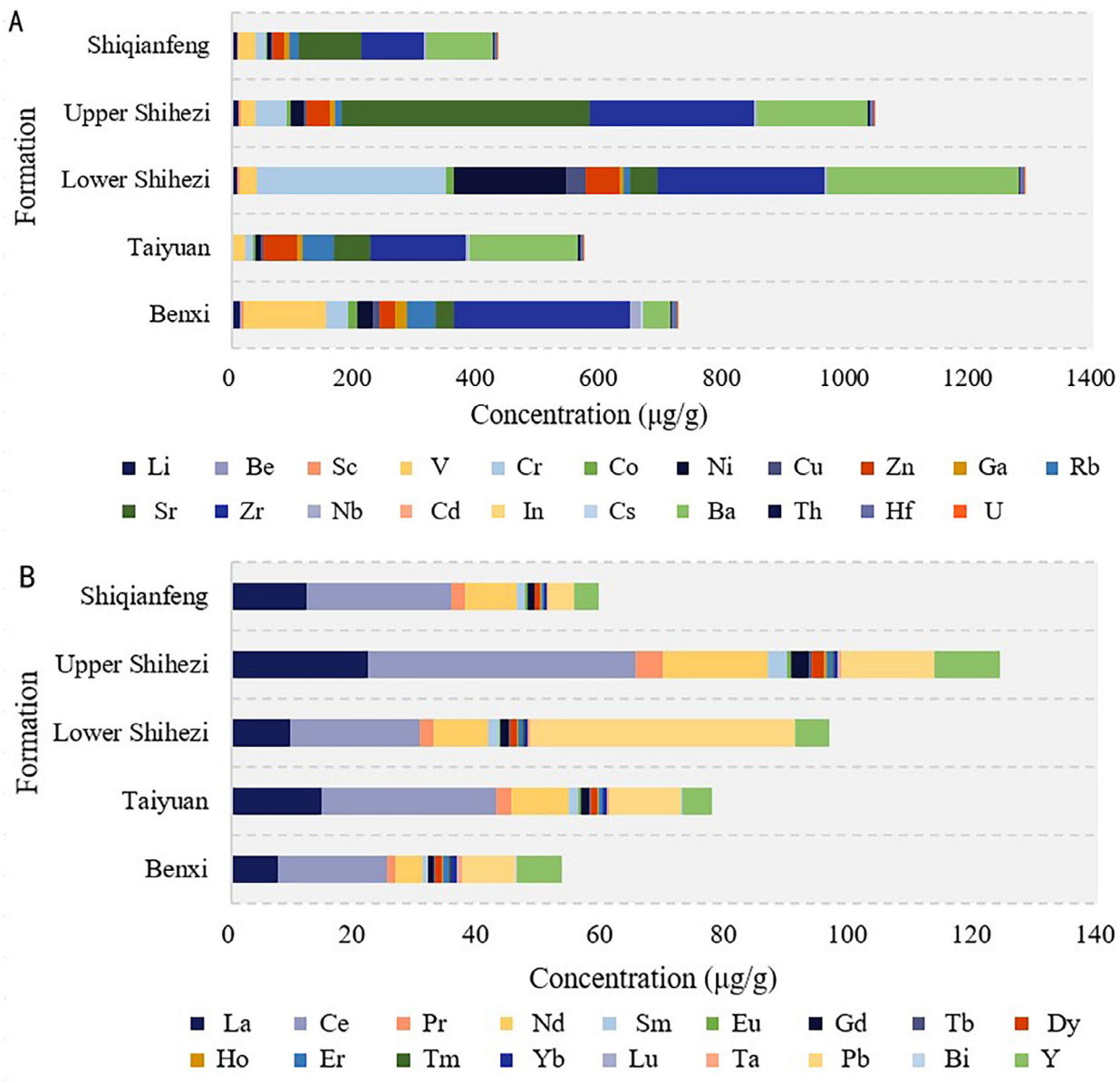


Figure 2. Element content distribution of the Shiqianfeng Formation–Benxi Formation. (A) Trace elements. (B) Rare earth elements.

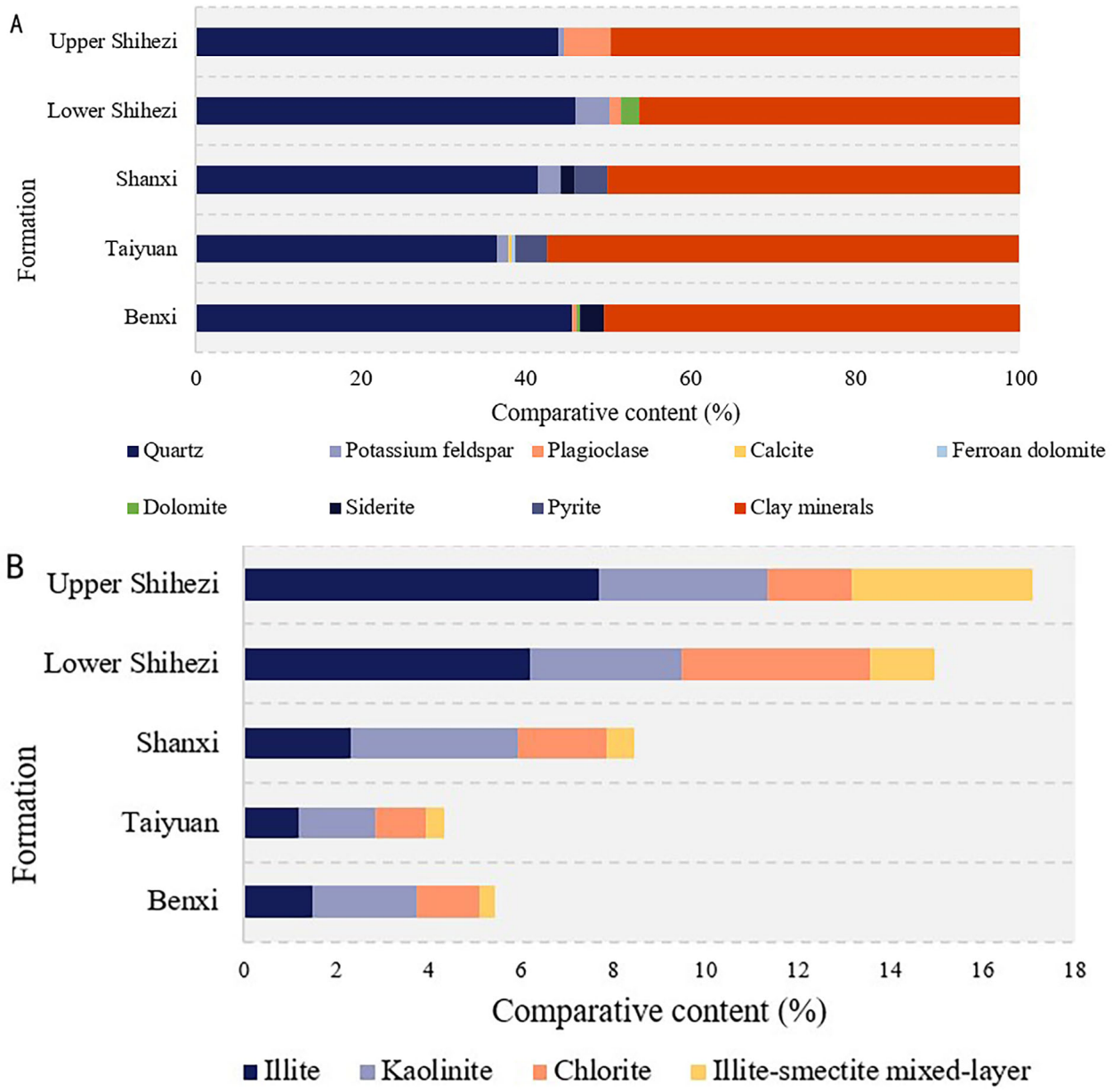


Figure 3. Mineral Composition of the Upper Shihezi Formation-Benxi Formation. (A) Bulk mineral composition of the samples. (B) Relative distribution of individual clay minerals within the total clay fraction.

log motifs. In the barrier island Taiyuan Formation, lagoon and swamp facies (containing coal and mudstone) corresponded to box-shaped and finger-shaped patterns, whereas tidal channel sandstones predominantly yielded a box-shaped signature. The carbonate mound facies, represented by thick marine bioclastic limestone, serves as a crucial indicator of a shallow epicontinental sea environment (Figure 4).

(ii) Facies correlation: Stratigraphic correlation based on wells LX-37, LX-34, LX-5, and LX-48 (Figures 5 and 6) indicated that the thickness of the Shanxi Formation was generally consistent. However, there was a local increase at well LX-5, which could be attributed to the development of deltaic lobes (comprising distributary channels and interdistributary bays). The Taiyuan Formation exhibits a thinning trend toward the center and thickening toward the margins, with coal seams being preferentially preserved in lagoon and swamp microfacies.

Analysis of sandbody orientation using image logs

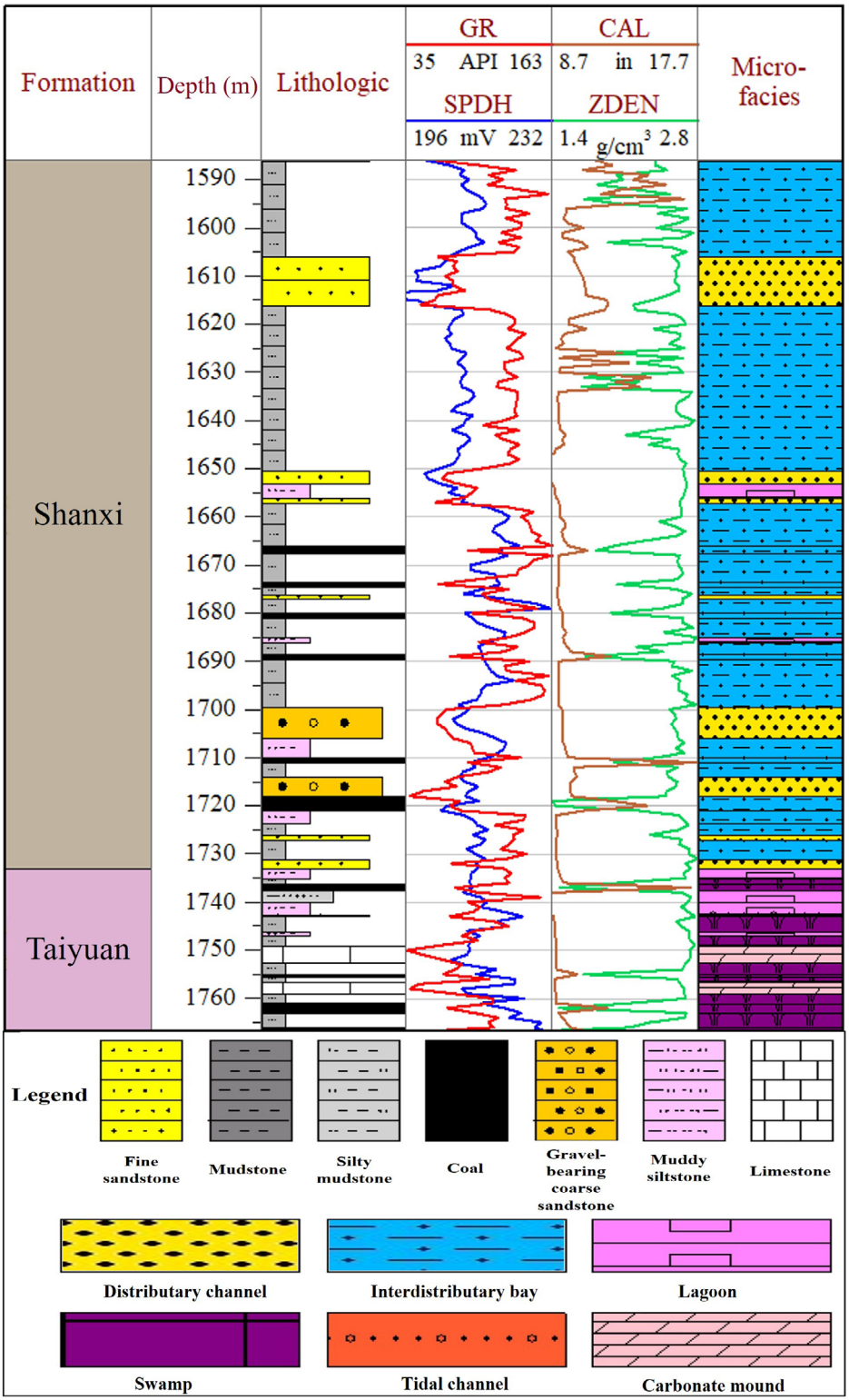


Figure 4. Comprehensive sedimentary facies map of the Shanxi Formation and Taiyuan Formation in well LX-5
Abbreviations: CAL: Caliper log; GR: Gamma-ray log; SPDH: Spontaneous potential from downhole tool with reference to a common remote electrode; ZDEN: Z-axis density log.

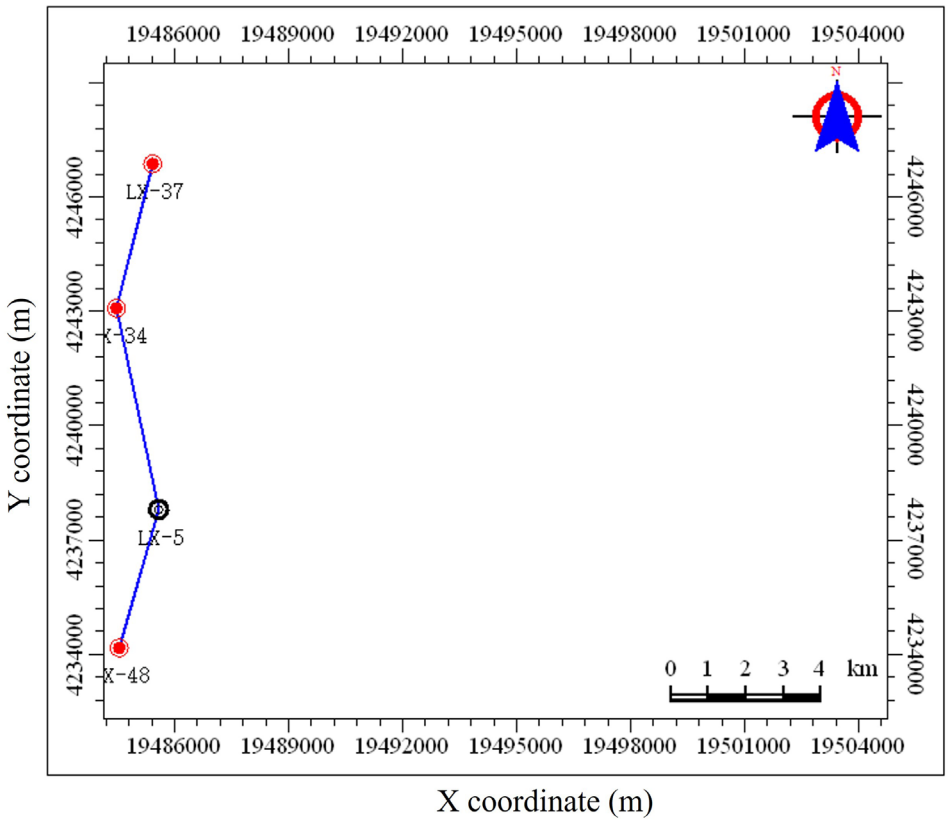


Figure 5. Location map of the well profiles from LX-37 to LX-48

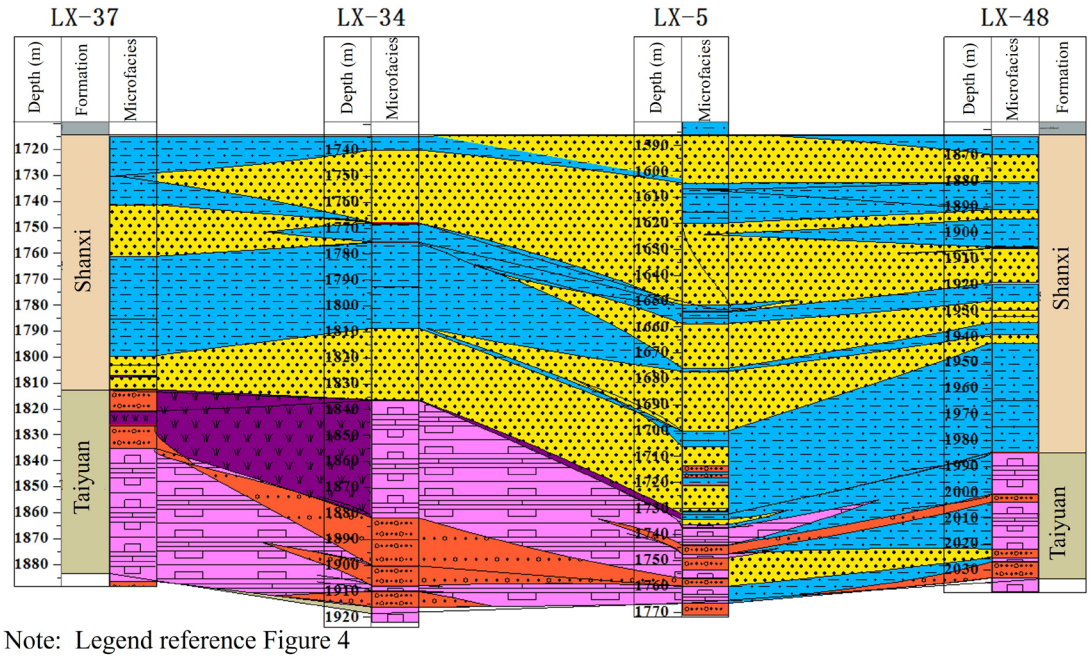


Figure 6. Sedimentary connected well sectional diagram of the LX-37 to LX-48 section

revealed that the primary paleocurrent direction of the Shanxi Formation was southward (locally northward), which confirmed a tide-dominated deltaic depositional environment with fluvial influence. The co-occurrence of high-energy sedimentary structures and significant coal seam thickness in the Taiyuan Formation collectively suggests deposition as a high-energy barrier island complex.

(iii) Planar facies distribution: Different seismic attributes have different sensitivities to sedimentary facies and lithology, and their prediction ability depends on the specific geological and geophysical characteristics of the study area. To objectively optimize the most sensitive attributes for the sedimentary microfacies of coal measure strata in this area, we first extracted six common attributes that may reflect lithology, physical properties, and structural characteristics based on geological knowledge: instantaneous amplitude, instantaneous frequency, instantaneous phase, sweetness, curvature, and root mean square (RMS) amplitude.

The optimization was based on two main aspects. First, from a geological–geophysical perspective, RMS amplitude reflects reflection intensity and is sensitive to the sandstone (high impedance)–mudstone (low impedance) interface, making it suitable for characterizing sandbody distributions, such as distributary channels and sand bars. The sweetness attribute, which combines amplitude and frequency, is often associated with high-porosity sandstone. Instantaneous phase highlights formation continuity and aids in tracing thin layers and lithologic boundaries. Instantaneous frequency is commonly related to formation absorption, attenuation, and tuning effects; however, in the strongly reflective coal-measure strata of this area, the strong absorption of high-frequency energy by coal seams may reduce the frequency information's resolution to lithological changes, resulting in limited predictive ability. Second, a well-seismic quantitative correlation analysis was performed. We calculated the statistical correlation between seismic attribute values and known sedimentary microfacies at key wells (LX-5). In this analysis, each depth point along the wellbore was assigned a microfacies label (categorical variable), and the corresponding attribute value at that depth was used for point-by-point correlation computation. The results show that RMS amplitude, sweetness, and instantaneous phase exhibited the strongest correlation with sandstone development degree and microfacies type, with correlation coefficients $r > 0.7$. In contrast, the curvature attribute exhibited a weak, unstable relationship with lithology/microfacies ($r < 0.3$), confirming its limited predictive capability in this dataset.

The threshold for the correlation coefficient was not a universal fixed standard, but an operational screening standard adopted for this study under specific dataset conditions. This empirical partition ($r > 0.7$ denoting "strongly correlated") highlighted the most predictive attributes, whereas the low correlation of curvature ($r < 0.3$) reflected its dataset-specific limitation. The threshold was therefore used primarily for attribute selection in this context, rather than as a general benchmark.

Consequently, based on the aforementioned geophysical principles and quantitative analysis, we optimized RMS amplitude, sweetness, and instantaneous phase attributes for subsequent attribute fusion and sedimentary facies modeling (Figure 7). The interpreted facies distribution revealed systematic seismic–geologic correlations: high RMS amplitude (red) was associated with distributary channels rich in sandstone; low amplitude (blue) corresponded to interdistributary bays filled with mud. In the Taiyuan Formation, distinct amplitude patterns distinguished the barrier island facies (high amplitude), tidal channel facies (medium-high amplitude), and lagoon facies (low-medium amplitude), as evidenced by the direct comparison between amplitude maps (Figure 7A,C) and facies maps (Figure 7B,D). The characteristic signature of the barrier island was ascribed to a strong impedance contrast at the sandstone-mudstone interface. These relationships emphasize the fundamental influence of acoustic impedance contrast on seismic amplitude in this context. Specifically, pure sandstone bodies produce high amplitudes, whereas clay-rich units produce low amplitudes.

4.2.2. Sedimentation environment evolutionary process

A multi-phase evolution of depositional environments is identified in the Upper Paleozoic sequence (Figure 8), reflecting changes in tectonic regime, paleogeography, and sediment source. (i) Late Carboniferous: Widespread marine transgression occurred, accompanied by the development of a barrier-coast lagoon system and the expansion of underwater distributary channels. (ii) Early Permian: Regional regression took place, with the development of barrier islands. The sedimentary environment was mainly dominated by the delta front. (iii) Middle Permian: The northern provenance weakened, and the sedimentary environment transitioned from a deltaic to a terrestrial lacustrine one, with the lake system gradually becoming the dominant feature. (iv) Late Permian: The sedimentary environment was dominated by terrestrial lake settings, with the extensive development of

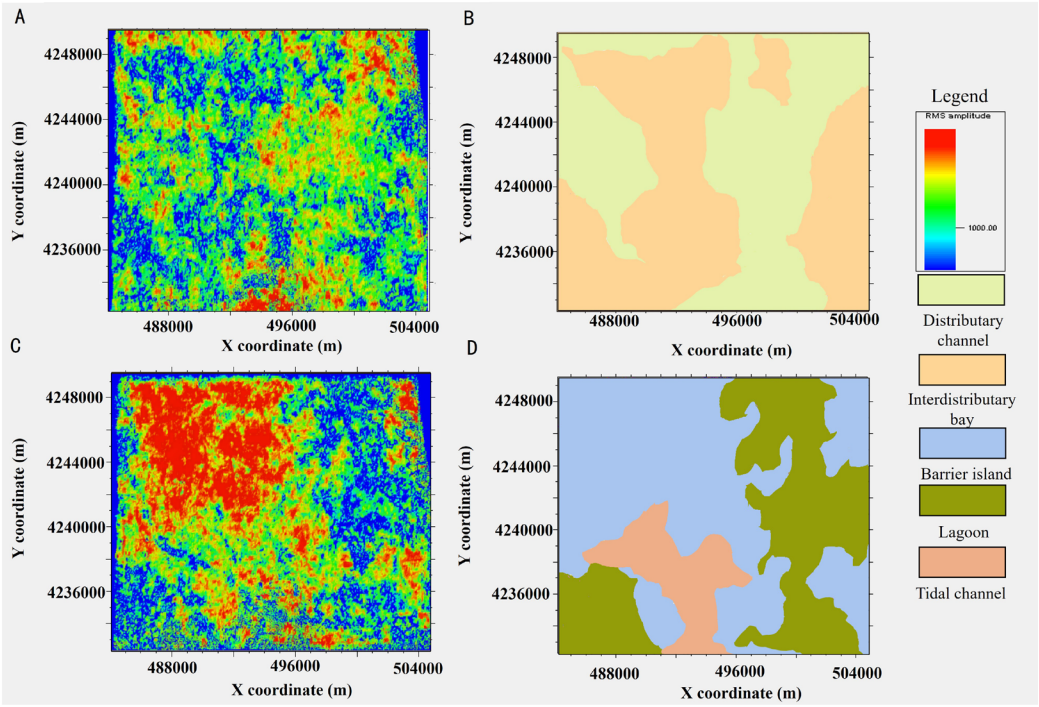


Figure 7. Root mean square (RMS) amplitude and sedimentary facies of the Shanxi Formation and the Taiyuan Formation. (A) RMS amplitude of the Shanxi formation. (B) Sedimentary facies of the Shanxi formation. (C) RMS amplitude of the Taiyuan formation. (D) Sedimentary facies of the Taiyuan formation.

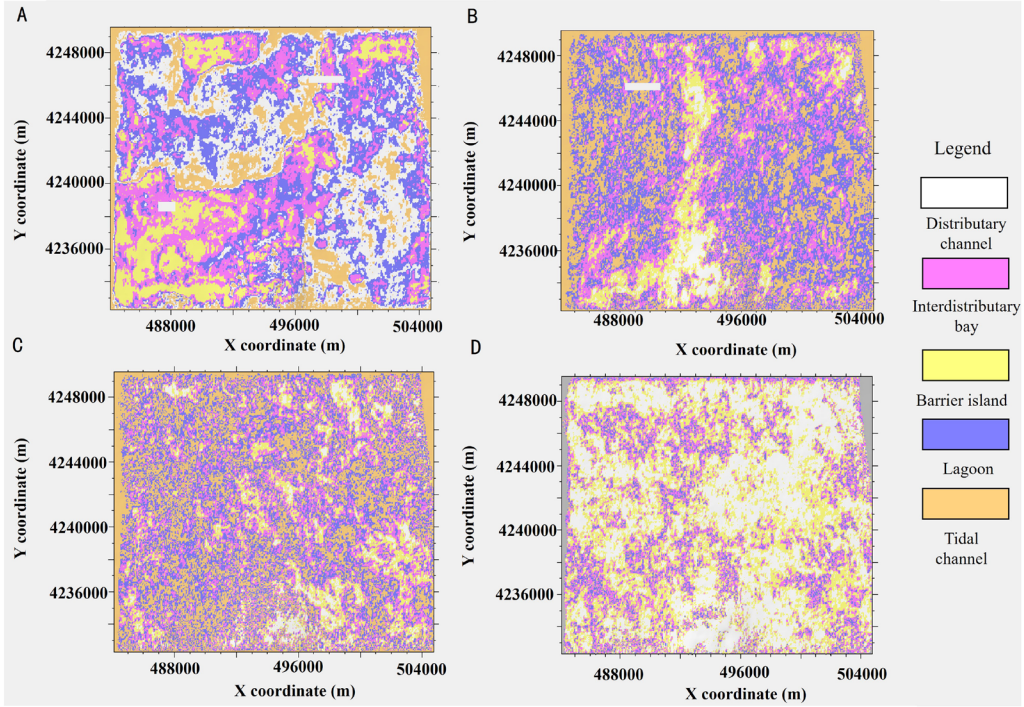


Figure 8. Evolution of the sedimentary environment. (A) Late Carboniferous epoch. (B) early Permian epoch. (C) Middle Permian epoch. (D) Late Permian epoch.

river deltas and shallow lakes.

4.2.3. The influence of the sedimentary environment on the differentiation of metal elements (Taiyuan Formation)

The enrichment level of elements was evaluated using the concentration coefficient (CC), defined as the ratio of an element's content in the studied coals to its average content in world coals.[36] According to the CC values, elements can be classified into four categories: enrichment ($5 < CC \leq 10$), slight enrichment ($2 < CC \leq 5$), normal ($0.5 < CC \leq 2$), and loss ($CC \leq 0.5$) (Figure 9).

The application of this scheme to the average metal content in the Shiqianfeng Formation–Benxi Formation of well LX-5 indicates that Zr exhibits enrichment; Cr, nickel (Ni), and hafnium (Hf) display slight enrichment; Li, scandium, vanadium (V), cobalt (Co), copper (Cu), zinc, Ga, rubidium (Rb), Sr, niobium, indium, cesium, Ba, and U are at background levels; while beryllium and cadmium show depletion.

For the study area's coal measures, paleoenvironmental conditions were reconstructed using combined petrographic, geophysical, and geochemical analyses. This discussion leverages that reconstruction to examine how sedimentary evolution influenced metal distribution. Table 2 presents the calculated trace element data for some LX-5 samples.

(i) Palaeosalinity (Sr/Ba): Sr/Ba ratios derived from key formations suggest a freshwater paleosalinity regime in the Taiyuan Formation (Figure 10). This geochemical evidence validates the interpreted tidal delta-barrier island environment, which underwent episodic marine incursions within a broader epicontinental sea context. The consequent extensive development of tidal and lagoon facies under such fluctuating salinity conditions fostered a reducing environment, thus facilitating the preservation of organic matter.

(ii) Palaeoclimate: The Sr/Cu ratio is a sensitive paleoclimatic indicator, reflecting the balance between elements for dry and wet conditions. Sr/Cu < 10 means a warm and humid climate, while Sr/Cu > 10 indicates a dry and hot climate.[37] The distribution of Sr/Cu values (Figure 11) shows that the Taiyuan Formation's sedimentary period was mainly warm and humid, consistent with it being a tidal delta barrier coastal sedimentary system in a land-surface sea environment. Additionally, variations in high and low S content of samples were investigated (Table 1). The Taiyuan Formation was mainly affected by terrestrial inputs and exhibited intermittent marine transgression features. Geochemical and sedimentary data together showed that paleoclimatic evolution, driven by sea-level fluctuations and changes in source supply, fundamentally controlled the geochemical signature of the coal measures.

(iii) Oxidation-reduction conditions: The distribution of redox-sensitive trace elements (e.g., V, Ni, Cr, U) in the samples is predominantly regulated by depositional redox conditions, as corroborated by their systematic variations across facies.[38,39] Table 3 presents an index for evaluating the redox environment of trace elements.

The V/Cr and Ni/Co ratios suggest that the overwhelming majority of samples were situated within an oxidizing environment. Merely a minuscule quantity of samples (e.g., L5-73) were in a weakly oxidizing-weakly reducing environment. In contrast, the L5-18 samples exhibited a reducing environment due to hydrothermal activity. A comprehensive analysis demonstrated that the sedimentary period in the study area was predominantly characterized by oxidative conditions, with a scarcity of typical and extensive reducing environments.

4.2.4. Explanation of the reduction signal contradiction

In this study, redox indicators showed a complex situation. Core observations of dark lithology, high TOC content, and widespread pyrite suggest a reducing depositional environment.[40,41], with geochemical ratios (e.g., V/Cr and Ni/Co) mostly indicating oxidation. This discrepancy implied that subsequent geological processes may have overprinted original sedimentary signals. The following possibilities were explored to explain these inconsistencies[39]:

(i) Yanshanian hydrothermal overprinting: Extensive Yanshanian tectonic-thermal events in North China might have altered original geochemical signals. Oxidizing and acidic hydrothermal fluids could have dissolved primary reducing minerals and introduced or modified elements, resetting V/Cr and Ni/Co ratios to suggest oxidative conditions.[42]

(ii) Terrestrial detrital dilution: The study area on the basin margin was affected by terrestrial input. Detrital minerals carrying Cr and Co diluted the authigenic signal of redox-sensitive elements, resulting in lower ratios and a false indication of an oxidative environment.[42]

(iii) Proxy limitations in multi-stage basins: Classic redox proxies like V/Cr and Ni/Co, established for marine shale, required careful assessment when applied to inland basins with complex diagenesis and multi-stage tectonic events. Multiple indicators should be used for verification in multi-cyclic basins.[42]

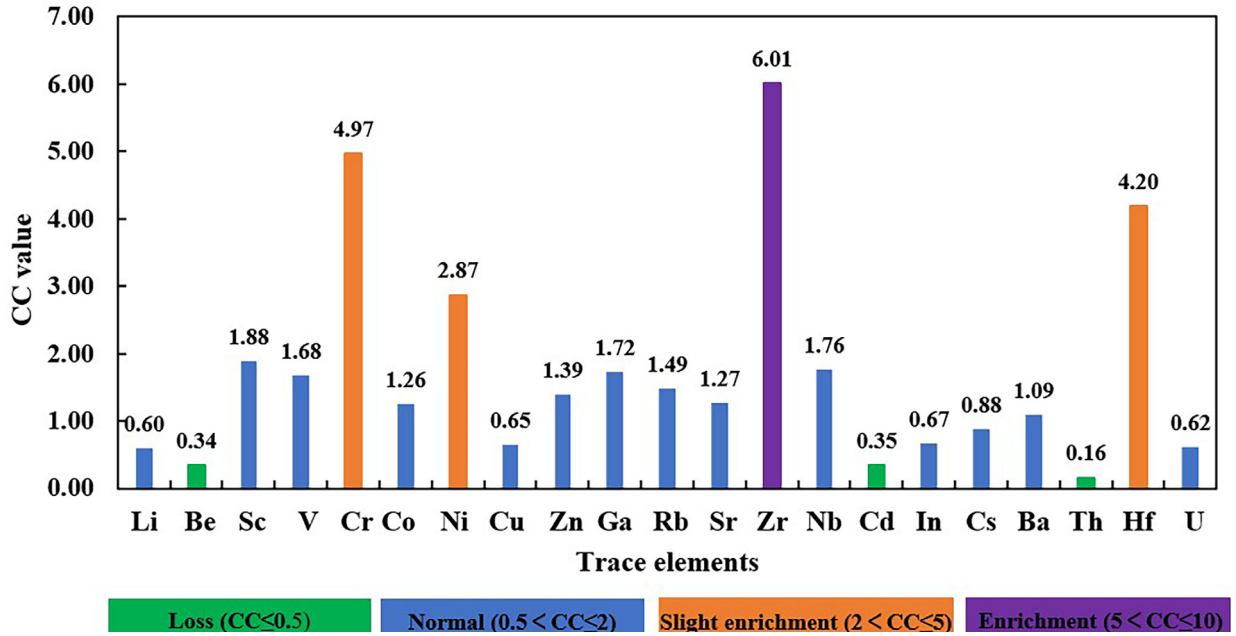


Figure 9. The calculated trace element concentration coefficient (CC) of the LX-5 well

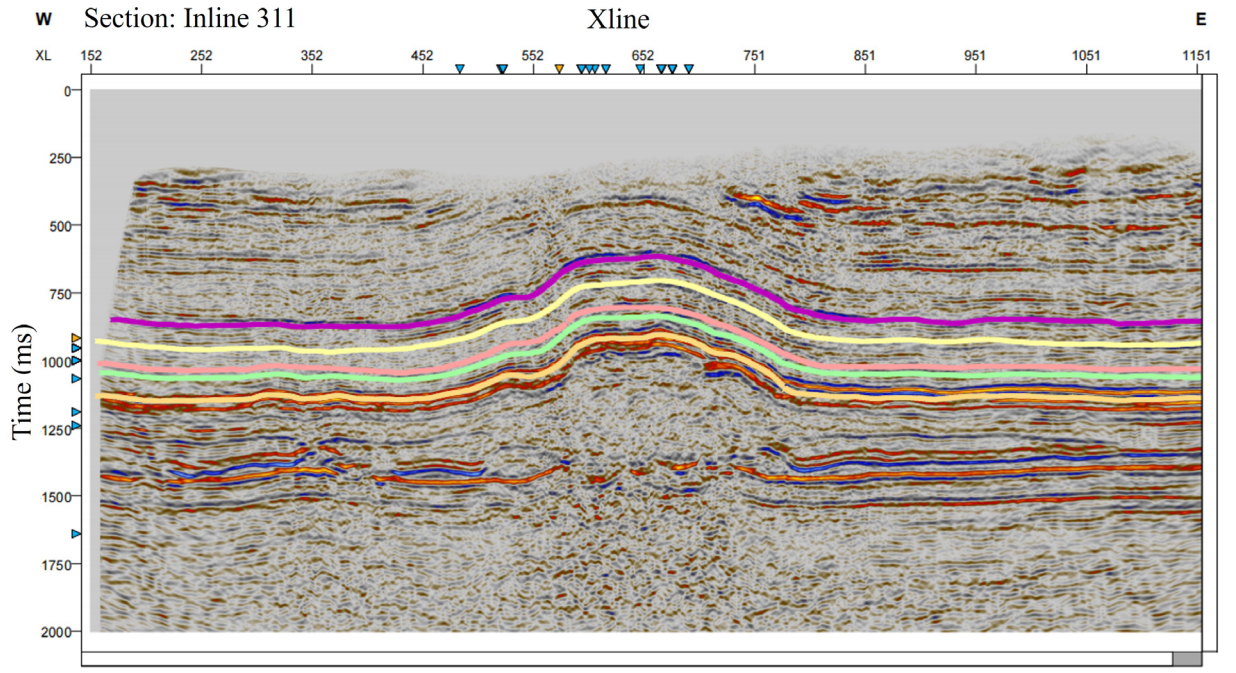


Figure 10. Seismic interpretation layer. Strata from the top to the bottom are: Shiqianfeng (P3s), Upper Shihezi (P2s), Lower Shihezi (P2x), Shanxi (P1s), and Benxi (C2b) formations.

Table 2. Trace element analysis calculation (μg/g)

Sample	Formation	Sr/Ba	Sr/Cu	V/Cr	Ni/Co	V/(V + Ni)	Co	Th/U
L5-7	Shiqianfeng	0.94	46.50	1.90	1.70	0.84	3.20	1.15
L5-11	Upper Shihezi	2.25	126.10	0.44	4.46	0.50	5.06	3.93
L5-18	Lower Shihezi	0.14	1.30	0.10	16.60	0.14	11.05	3.52
L5-22	Taiyuan	0.34	16.30	1.48	2.19	0.71	3.66	3.12
L5-73	Benxi	0.63	2.50	3.78	1.67	0.84	14.71	5.15

Abbreviation: Ba: Barium; Co: Cobalt; Cu: Copper; Ni: Nickel; Sr: Strontium; Th: Thorium; U: Uranium; V: Vanadium.

Table 3. Trace elements redox environment judgment index

Trace element	Reduction	Weak oxidation–weak reduction	Oxidation
V/Cr	>4.25	2.00–4.25	<2
Ni/Co	>7.00	5.00–7.00	<5

Abbreviations: Co: Cobalt; Cr: Chromium; Ni: Nickel; V: Vanadium.

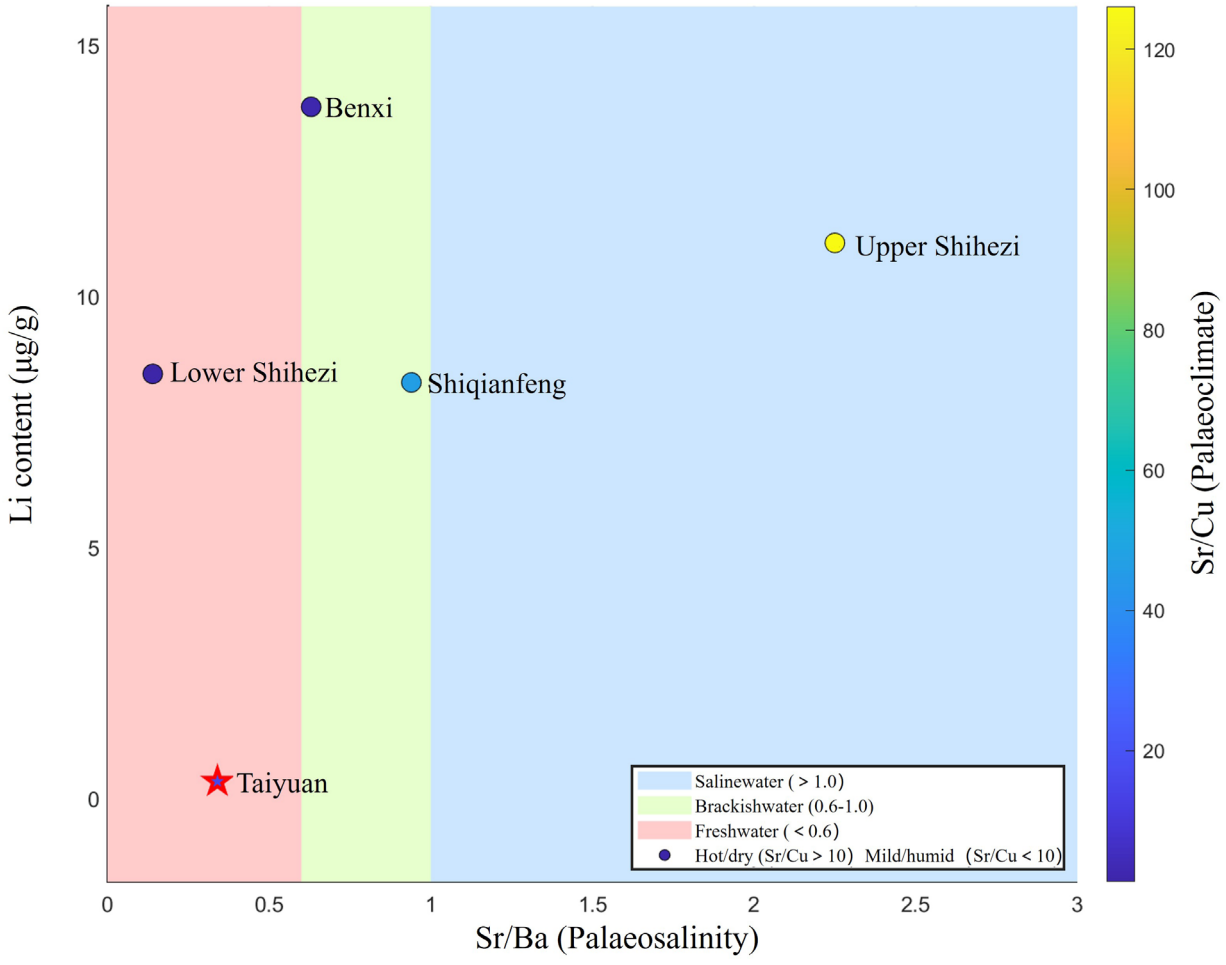


Figure 11. The distribution of lithium (Li), strontium (Sr)/ barium (Ba), and Sr/ copper (Cu)

Based on the evidence, the Taiyuan Formation coal seams formed in an anoxic environment during sedimentation and early diagenesis, which is favorable for organic matter preservation and pyrite formation. However, subsequent hydrothermal activity (likely Yanshanian) modified the original geochemical features. Thus, primary sedimentary environment information from core observations and TOC is more reliable than potentially modified elemental ratios.

4.2.5. Multi-factor control on metal enrichment

Integrated analyses demonstrated that the sedimentary environment of the Taiyuan Formation had multi-factor control on metal differentiation. Facies analysis indicated that the Taiyuan Formation developed diverse facies, including lagoon and tidal-flat settings, whereas the overlying Shanxi Formation had a homogeneous, river-dominated delta system. Paleosalinity and lithofacies, combining with trace-element indicators, suggest that the Taiyuan Formation was deposited in a tidal delta-barrier island system in an epicontinental sea. This freshwater-dominated system, interrupted by transgressions, enabled the preservation of organic matter and the development of reducing conditions. The paleoclimate was warm and humid, and together with high S content and peat swamps, it enhanced the stability of the reducing interface. The reducing environment of the Taiyuan Formation regulated the evolution of organic matter and influenced metal enrichment through sulfidation and organometallic complexation.

4.3. Tectonic thermal events

4.3.1. Balanced cross-section

The construction of balanced cross-sections depends on quantitative erosion (acoustic time-difference method) and on reconstructing the burial history. Integrating interpreted seismic horizons (from the Heshanggou Formation to the Benxi Formation) (Figure 10) and well-based depth conversion indicates a structure modified by uplift and erosion. Therefore, a balanced cross-section (Figure 12) was constructed by restoring the missing section, decompacting strata, and sequentially removing fault displacement and folding.

The tectonic history of the study area was defined by a multi-phase evolution with major unconformities (Figure 12). It began with the deposition of Ordovician carbonate platform sediments in the early Paleozoic. The Caledonian Orogeny ended this phase, causing uplift and significant erosion that removed Silurian and Devonian strata. Then, in the late Paleozoic, Variscan-influenced subsidence allowed the deposition of Carboniferous–Permian coal measures and overlying Permian–Triassic clastic rocks on the truncated Ordovician basement. Triassic burial compacted the coals rapidly under stable conditions. In the Mesozoic, a major tectonic inversion occurred. The Indosinian and Yanshanian orogenies led to the early Cretaceous uplift of the Zijinshan belt, compression, reactivation of fault systems, and erosion of Jurassic–Cretaceous deposits. A weak extensional regime then stabilized the structure. Finally, from the Cenozoic to the Quaternary, there was tectonic quiescence, with thin Tertiary and Quaternary sediments covering the eroded Triassic landscape.

4.3.2. Zijinshan pluton

The Late Jurassic to Early Cretaceous period was characterized by intense magmatism, as exemplified by the Zijinshan pluton in the southern study area. This intermediate-to-deep intrusive-extrusive complex intruded the Lower Paleozoic Majiagou Formation. Remnants of carbonate roof pendants and overlying Carboniferous–Permian strata showed their post-Paleozoic emplacement (Figure 13).

This magmatic activity affected metal endowment through a multi-faceted process. A high geothermal gradient around the Zijinshan pluton indicated a thermal anomaly, which accelerated organic matter maturation in adjacent coal measures and raised vitrinite reflectance in the Benxi Formation to 0.978–1.654% (Table 1). Then, magmatically derived hydrothermal fluids circulated through the sequence, transporting, introducing, and enriching (or depleting) trace metals in coal seams.[43–46]

Moreover, the emplacement dynamics created abnormal fluid pressures, forming and reactivating fracture networks in multiple stratigraphic units. Later-stage volcanic eruptions increased permeability by dilating fractures and creating secondary cracks. These structures were the main conduits through which metal-laden hydrothermal fluids entered coal-bearing strata, especially along fault zones and volcanic conduits.

4.3.3. Fluid inclusion constraints on hydrothermal activity

Microthermometric analysis of fluid inclusions from quartz grains in the Shanxi Formation sandstones of well LX-5 showed direct constraints on the nature and timing of hydrothermal activity. Two populations of secondary aqueous inclusions were identified, hosted within healed micro-fractures and dissolution pores. They recorded distinct thermal events: an earlier, lower-temperature phase (Event I: Th 92.8–185.7 °C) and a later, dominant moderate-temperature phase (Event II: Th 104.7–183.2 °C), both exhibiting moderate to high salinities (6.74–12.96

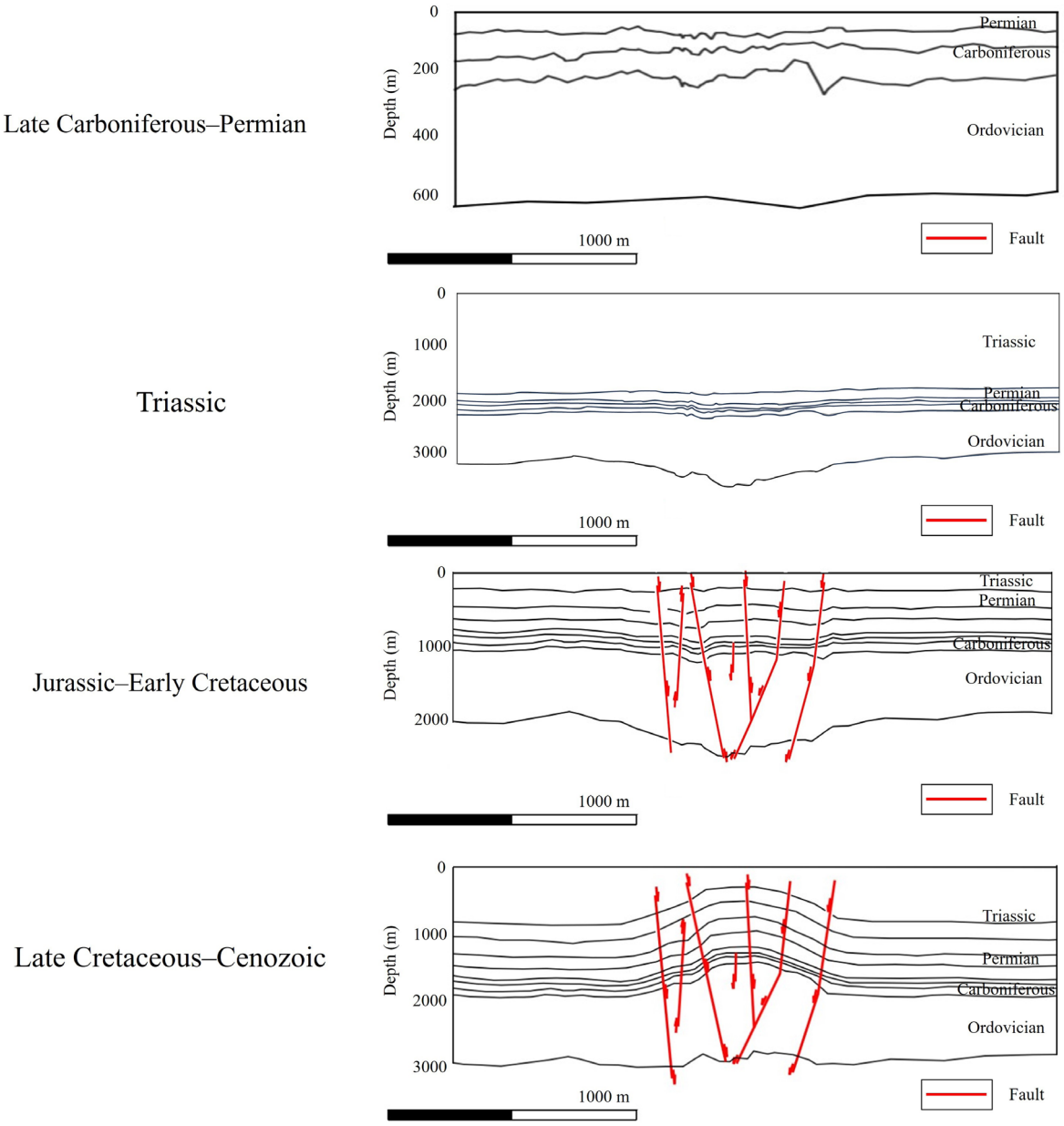


Figure 12. Tectonic evolution process in the study area based on the balanced cross-section technique

weight % sodium chloride equivalent). The temperature range of Event II aligned with the moderate-temperature hydrothermal regime independently inferred from elevated vitrinite reflectance and REE signatures. Critically, the secondary nature of these inclusions, their textural association with late-stage fractures, and their moderate-temperature–moderate-salinity characteristics collectively indicated that the entrapped fluids were genetically linked to the Yanshanian tectono-thermal event rather than to earlier diagenetic or later unrelated fluid episodes. This evidence reinforces that fault and fracture networks acted as primary conduits for metal-bearing hydrothermal fluids during the Yanshanian, thereby explaining the post-depositional remobilization and localized enrichment of critical metals such as Cr.

4.3.4. Mechanisms and controls of critical metal enrichment in coal strata

The enrichment of critical metals in coal strata is attributed to the coupled effects of recurrent magmatism and exhumation. This coupling occurs through distinct but complementary processes: (i) Syn-depositional fault

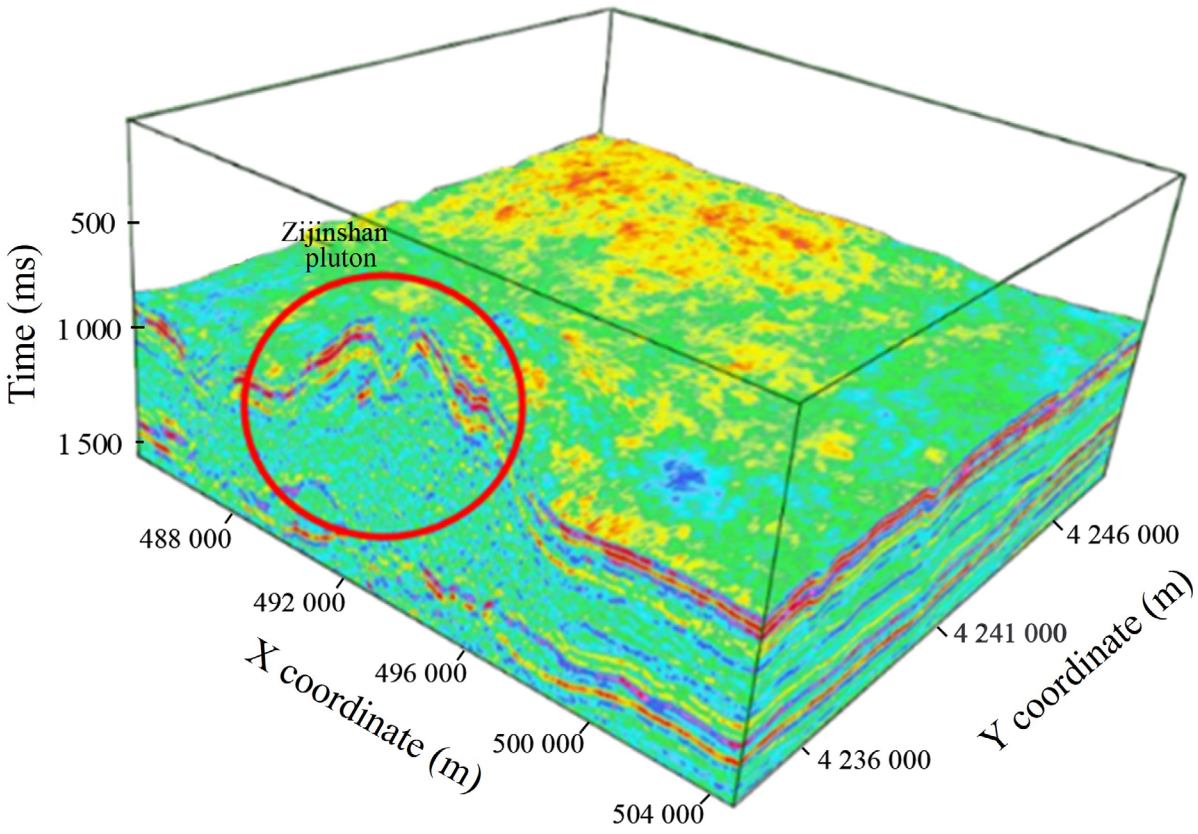


Figure 13. Three-dimensional visualization of Zijinshan pluton interpretation

Table 4. Summary of fluid inclusion data by event

Event	Number of inclusions	Homogenization temperature range (°C)	Mean temperature (°C)	Salinity range (weight %)	Mean salinity (weight %)	Main occurrence	Host mineral
Event I	10	92.8–185.7	131.67	8.41–10.61	9.56	Fissure	Quartz
Event II	10	104.7–183.2	145.22	6.74–12.96	9.94	Fissure, dissolution	Quartz

networks, activated by the Zijinshan pluton, promoted topographic differentiation and concentrated the vertical migration of deep ore-bearing fluids, resulting in metal deposition at permeability barrier islands within the coal sequence; (ii) The direct influx of hydrothermal fluids containing Au, Cu, and REEs facilitated alteration assemblages (e.g., kaolinite), as evidenced by elemental anomaly studies.

The significance of integrating multiple controlling factors is exemplified by the LX-5 well, situated in a tectonically stable area far from volcanic centers. Its distinct trace element and REE patterns, in contrast to those in the volcanically influenced zone, cannot be explained solely by the structural history. This geochemical disparity conclusively indicates that an effective prediction of metal-enrichment heterogeneity requires a model that simultaneously accounts for sedimentary facies distributions and the influence of paleo-groundwater systems.

4.4. Groundwater distribution

The distribution and flow of groundwater, which are regulated by stratigraphic porosity and permeability, tectonic fractures, and hydrological gradients, served as the primary medium for the activation, migration, and reprecipitation of critical metals. The subsequent analyses reconstructed the paleogroundwater system and delineated its specific roles in metal enrichment.

4.4.1. Wave impedance inversion

This study used wave impedance inversion technology to identify high-porosity and high-permeability sandstone bodies (e.g., distributary channels and sand dams) by precisely characterizing subsurface lithology wave impedance differences. Such sandstone bodies are favorable for controlling critical metal migration and enrichment in coal measures; thus, the inversion results directly contribute to predicting the spatial distribution of critical metals.

Traditional inversion methods are limited by wavelet and model constraints.[47,48] Recent deep learning approaches, particularly generative adversarial networks (GANs), enhance automation and resolution by learning nonlinear seismic-impedance mappings.[49] Unsupervised physics-driven networks[50] and GAN-based data augmentation methods[51] further enhance the robustness of the methods under limited samples.

The wave impedance value was obtained by natural gamma pseudo-acoustic inversion. The black-lined low-value green area was sandstone, and the rest was mudstone. The low-impedance zone (green) in Figure 14 was highly consistent with the sandstone development zone interpreted from logging, confirming its reliability. These confined low-impedance sandstone bodies, with high porosity and permeability, are interpreted as fluid-dominant channels for the migration and enrichment of metal elements, including Cr, Ni, and Zr, providing key geophysical evidence for constructing a tectonic-sedimentary fluid-joint ore-control model.

4.4.2. Property–structural coupled model

Model construction and integration used geostatistical simulation of log data to construct 3D porosity-permeability models, which were overlaid on structural maps (Figures 15 and 16). Comparative analysis with the sedimentary facies model (Figure 7) indicated that high-quality reservoir zones corresponded spatially with distributary channel and tidal bar sand bodies, suggesting depositional facies controlled primary pore development. Structural elements, especially faults in the Zijinshan pluton, further conditioned these properties. High-porosity regions often correlate with structural highs and are inferred as groundwater conduits.[52] Fault-mediated enhancement varies by lithology, improving sandstone porosity and fracturing muddier units. This synthesis of sedimentological and structural controls forms the basis for a two-factor reservoir evaluation model.

The property–structural coupled model is relevant to critical metal enrichment as porosity and permeability control hydrothermal fluid flow in the coal-bearing sequence. High-porosity and high-permeability zones (e.g., distributary channel sand bodies) are preferential conduits for metal-bearing fluids, while low-permeability mudstone layers can act as seals. Faults and fracture zones within the structural coupling are critical fluid pathways that connect deep-seated metal sources to reservoir rocks. Thus, the coupled spatial distribution of porosity, permeability, and the structural framework provides a predictive model for critical metal sweetness, which underpins the interpretation of observed metal distribution patterns.

4.4.3. Groundwater leaching and weathering

An anomalously high Th/U ratio (>7) is typically due to groundwater leaching under strong oxidation. However, hydrothermal fluids can also leach and transport U, leading to U loss and increasing the Th/U ratio. The Co content can be used for auxiliary discrimination, as hydrothermal activity can lead to significant Co enrichment. The Th/U ratios of all samples were calculated (Figure 17) to identify samples with anomalously high (>7) or low (<2) values. The H-35 sample of Upper Paleozoic mudstone had a Th/U value of 39.43, indicating strong oxidation and groundwater leaching.

These data showed that source-area rocks generally weather highly, and leaching by atmospheric freshwater could enrich and differentiate REEs in source-area granite. By combining the Th/U ratio and Co trace-element data, a comprehensive interpretation was made to clarify the combined control of redox conditions, groundwater leaching, and hydrothermal activity.

4.4.4. Reconstruction of the paleo-groundwater system and its role in key metal enrichment

This section reconstructed the paleo-groundwater system in the study area via wave impedance inversion, attribute–structure coupling modeling, and geochemical index analysis, and disclosed its core function in the activation, migration, and reprecipitation of key metals. The findings indicate that the enrichment of key metals results from sedimentation-structure-fluid coupling, deepening understanding of the mineralization of coal-measure key metals.

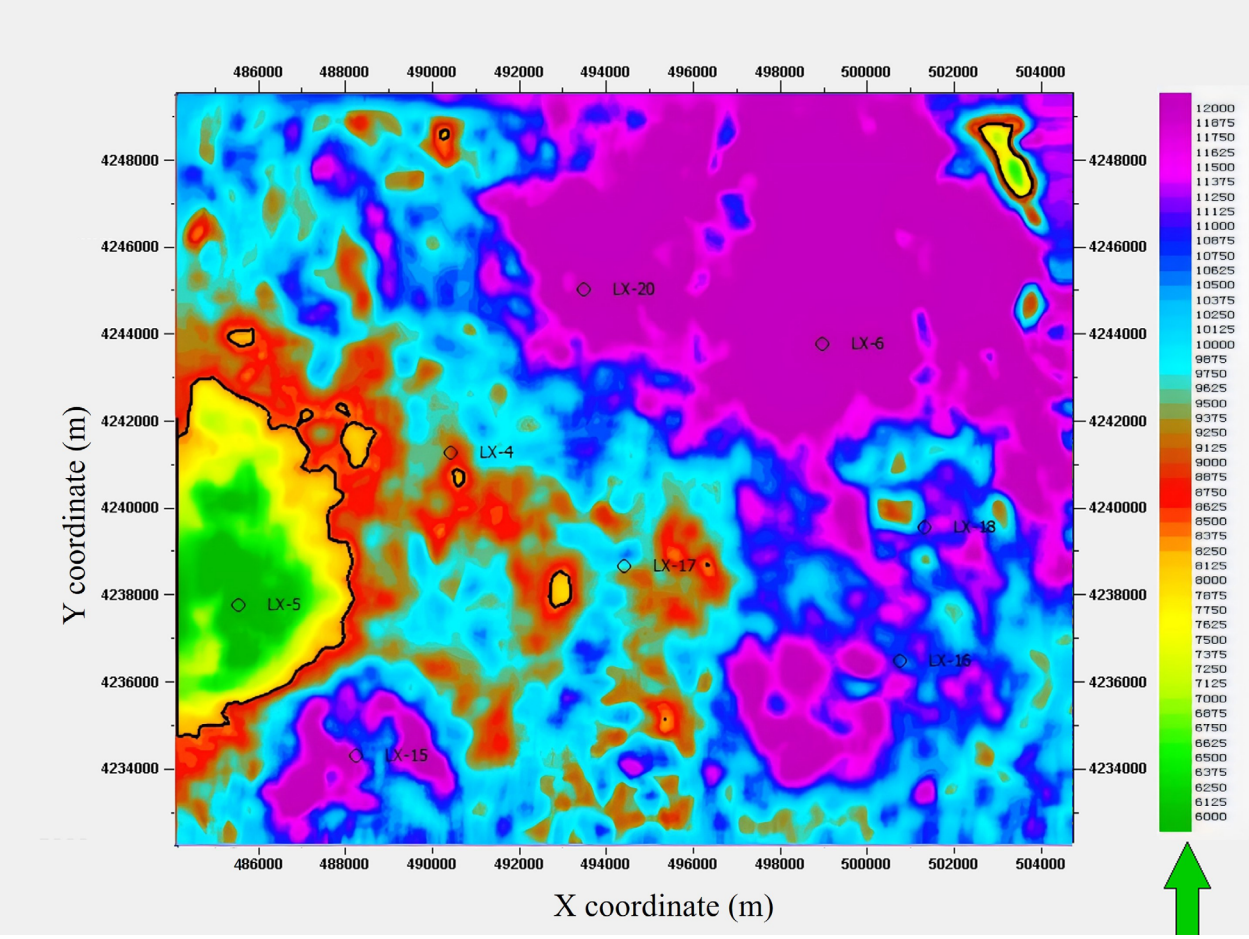


Figure 14. 4 + 5 # coal seam (a major coal seam within the coal-bearing strata of the study area characterized by relatively thin thickness with significant lateral variation) roof lithology

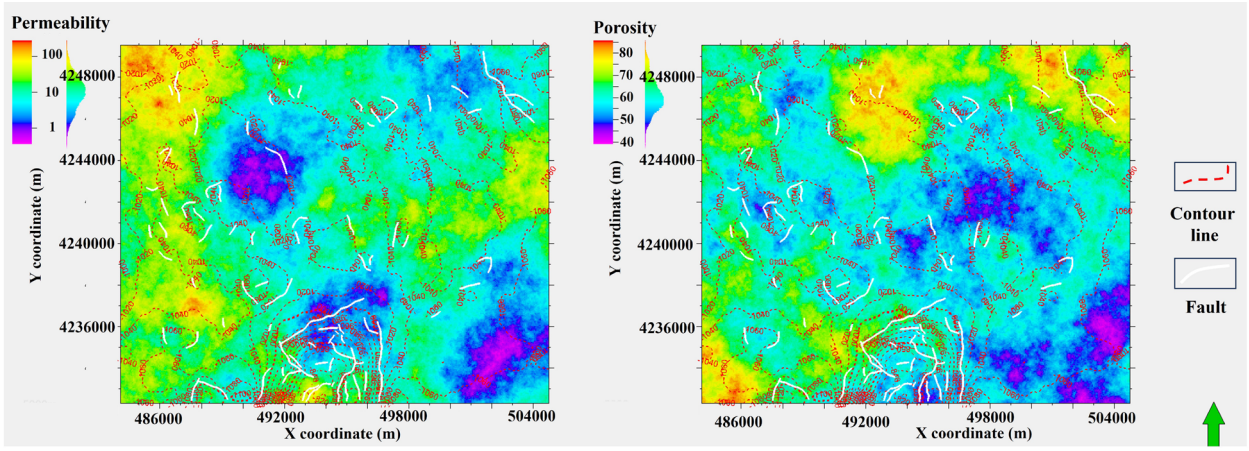


Figure 15. Comprehensive property–structural coupled model map of the Shanxi Formation

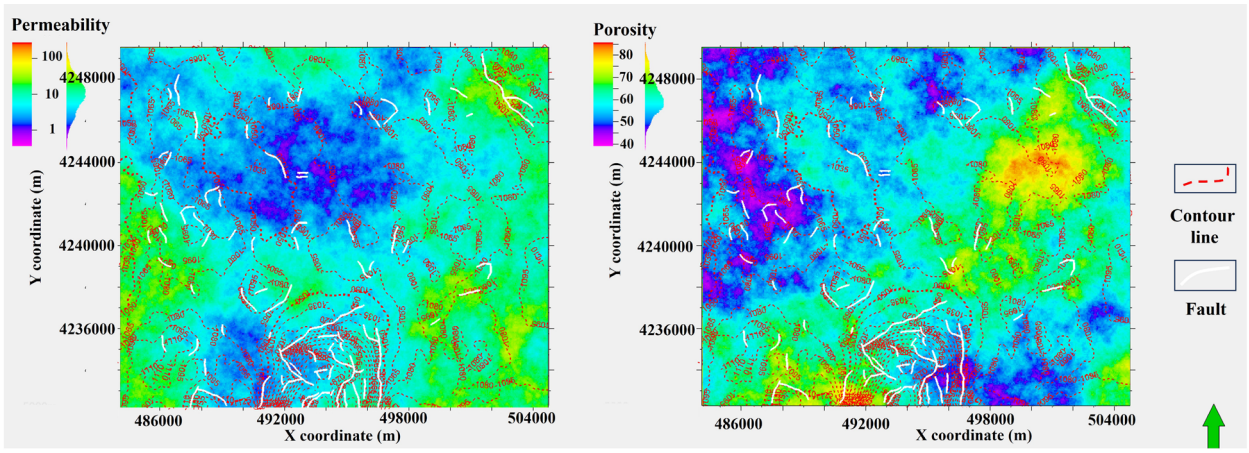


Figure 16. Comprehensive property–structural coupled model map of the Taiyuan Formation

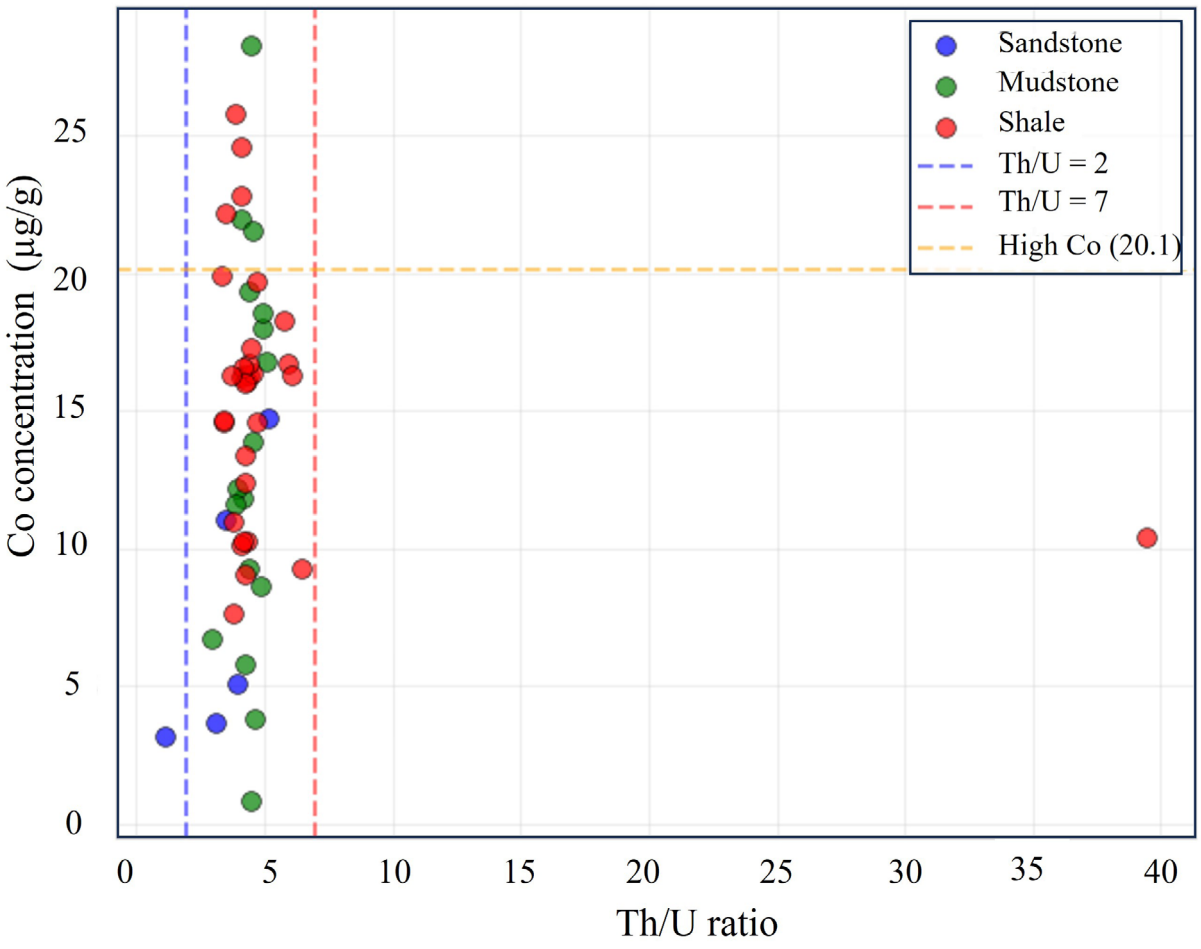


Figure 17. The thorium (Th)/uranium (U) ratio and cobalt (Co) content distribution of the samples

Firstly, wave impedance inversion identified sandstone bodies with high porosity and permeability, consistent with the reservoirs interpreted from well-logging data. These sandstone bodies serve as "preferential channels" for the migration of metal elements, offering evidence for the structure–sedimentation–groundwater joint ore-controlling model and establishing a connection between sedimentary pore networks and fluid transport pathways.

Secondly, the attribute–structure coupling model realized 3D quantitative characterization of the porosity-permeability field. High-quality reservoir areas were correlated with sedimentary facies, validating that sedimentary facies were the foundation for the development of primary pores. Tectonic activity modified the sedimentary framework, forming a pattern of sedimentary control and structural alteration of storage. The coupling of the porosity-permeability field and the structural framework formed the physical basis for predicting key metal "sweet-spot areas" and accounted for the distribution of metals.

Finally, geochemical tracing of groundwater leaching and weathering provided evidence of fluid-rock interactions for the physical model. An abnormal Th/U ratio indicated groundwater leaching under strongly oxidizing conditions. By analyzing trace elements such as Co, the effects of atmospheric freshwater leaching and hydrothermal activity can be discriminated. These data demonstrate that source-area rocks have experienced intense weathering, and atmospheric freshwater leaching enriches and differentiates REEs. This clarifies the chemical properties of the paleo-groundwater and integrates fluid-chemical reactions with physical transport channels.

4.5. Comprehensive control factors of metal distribution

The fault and fracture network generated by the Yanshanian tectonic thermal events (particularly those associated with the Zijinshan rock mass) not only functioned as a crucial conduit for hydrothermal fluids but also fundamentally remodeled the flow path of paleo-groundwater systems, significantly enhancing the stratum's permeability. These structurally controlled permeable zones directed the flow of paleo-groundwater (comprising atmospheric precipitation and deep-basin fluids) and formed and governed the position of redox fronts at the interfaces between highly permeable sandstone bodies (e.g., distributary channels) and low-permeability mudstone interlayers, or at different lithological/fluid contact zones.

The reactivation, migration, and ultimate precipitation of metals resulted from the combined effect of structural channels and porosity/permeability fields controlled by sedimentary facies. Specifically, deep hydrothermal and basin fluids migrated upward along faults (under structural control), then laterally in high-porosity sandstone bodies determined through sedimentary facies (under sedimentary control), and finally precipitated at the redox front located via structural uplift or lithological traps (under the joint control of structure, sedimentation, and fluid).

This joint-control model of structure, sedimentation, and groundwater effectively linked deep-seated hydrothermal events with shallow-fluid redistribution processes, thereby elucidating the causes of spatially heterogeneous metal enrichment.

4.6. Enrichment mechanism of chromium

To clarify the enrichment mechanism of critical metals in the eastern margin of Ordos Basin, Cr was selected for in-depth analysis. The reasons were as follows: First, CC indicated that Cr was slightly enriched in the study area, much higher than the background value, making it suitable for exploring metal enrichment. Second, Cr showed a specific enrichment in the Lower Shihezi Formation, providing a good opportunity to analyze geological factors, such as sedimentary environment, tectonic activity, and fluid migration. Thus, this study aims to establish a widely applicable source–transport–storage model by analyzing Cr's enrichment mechanism, applicable not only to Cr but also to other enriched critical metals such as Zr, Ni, and Hf in this area.

4.6.1. Provenance analysis

Chromium distribution within the Carboniferous–Permian succession revealed a distinct enrichment anomaly in the Lower Shihezi Formation (Figure 18).

In geochemistry, Cr is usually closely associated with ultrabasic and mafic rocks, such as basalt and serpentinite suites. Its enrichment in sediments may indicate the contribution of basic volcanic rocks, gabbro, or metamorphic basic rocks in the source area. Cr can also occur in heavy minerals, such as chromite, and provides a good source tracer. Data on Taiyuan Formation coal-bearing shale and Upper Paleozoic mudstone from previous studies were selected[12,40], and the correlation among Cr content, aluminium oxide (Al_2O_3), and potassium oxide (K_2O) in the samples was poor (Figure 19). Cr and V (with a high correlation coefficient), Ni, Co, and other siderophile elements often exhibit good positive correlation (Figure 20). The abnormally high Cr content, no significant correlation between Cr and Al_2O_3 and K_2O, and a strong correlation between Cr and V and Ni suggest that they may jointly originate from weathering products

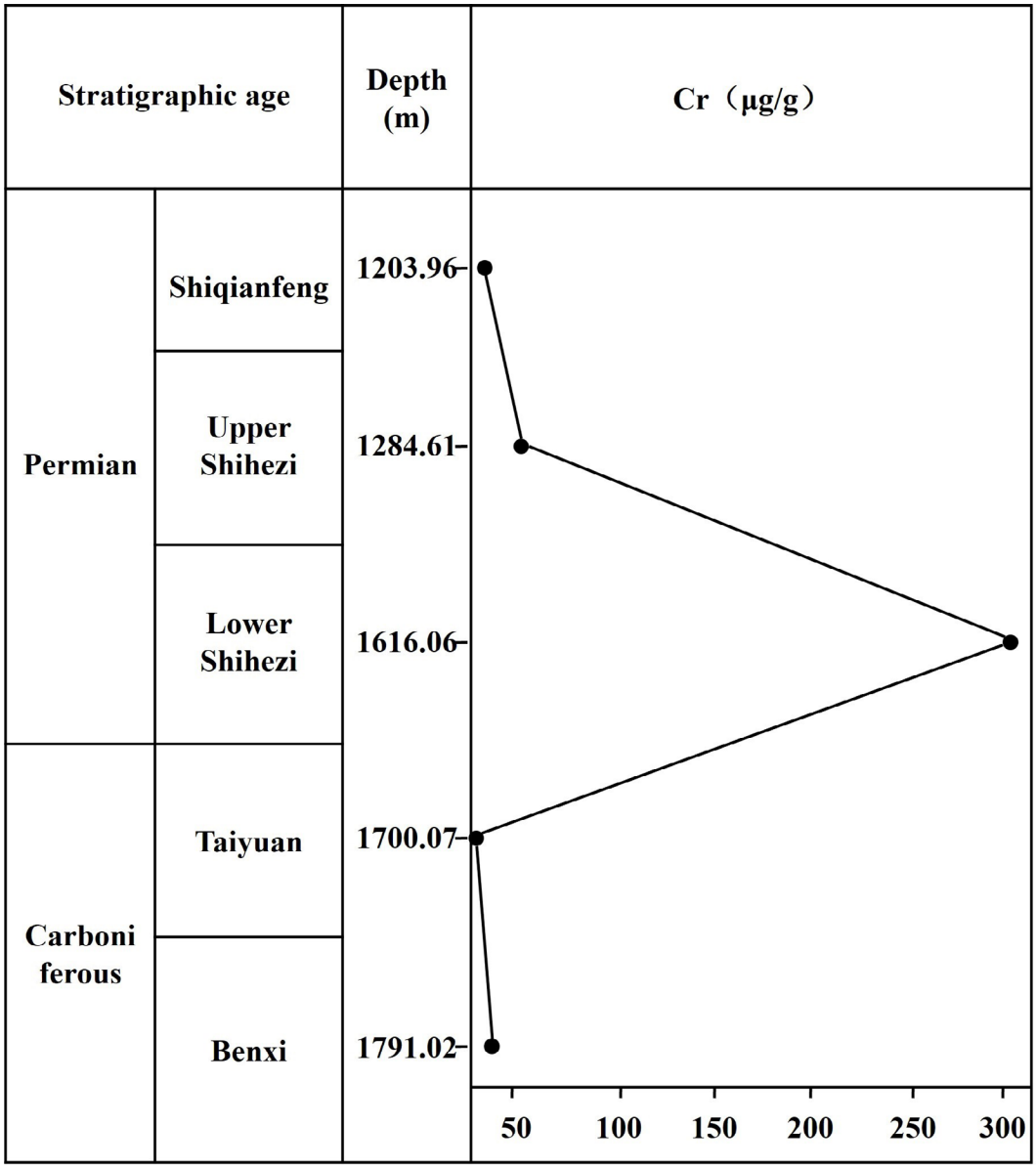


Figure 18. The distribution of chromium (Cr) element content

of basic/ultrabasic rocks (such as gabbro and peridotite), or be related to volcanic materials and hydrothermal activity.

The main source of Cr in coal in the study area is terrestrial debris rich in basic/ultrabasic rock components. These rocks are rich in primary minerals, such as chromite and chromite silicates. Important local sources include hydrothermal activity and volcanic ash. For the anomaly point L5-18 (sandstone), its extremely high Cr content and Cr/Th ratio, as well as the possible existence of special lithology or sedimentary structures in this layer, strongly suggest hydrothermal fluid activity during the same or quasi-same sedimentary period, or direct deposition of basic volcanic ash. Sandstone, as a highly permeable rock layer, is more likely to become a hydrothermal channel. Part of Cr may be adsorbed onto Fe oxides or bound to organic matter, but these processes are not the dominant factor.

4.6.2. Distribution mode of rare earth elements

The source of REE was determined using the anomalies of Eu, Ce, lanthanum (La), yttrium (Y), and holmium (Ho), with the formula as follows (**Equations 1–3**):

$$\delta Eu = \frac{Eu}{Eu^*} = \frac{Eu_N}{\sqrt{Sm_N \times Gd_N}} \quad (1)$$

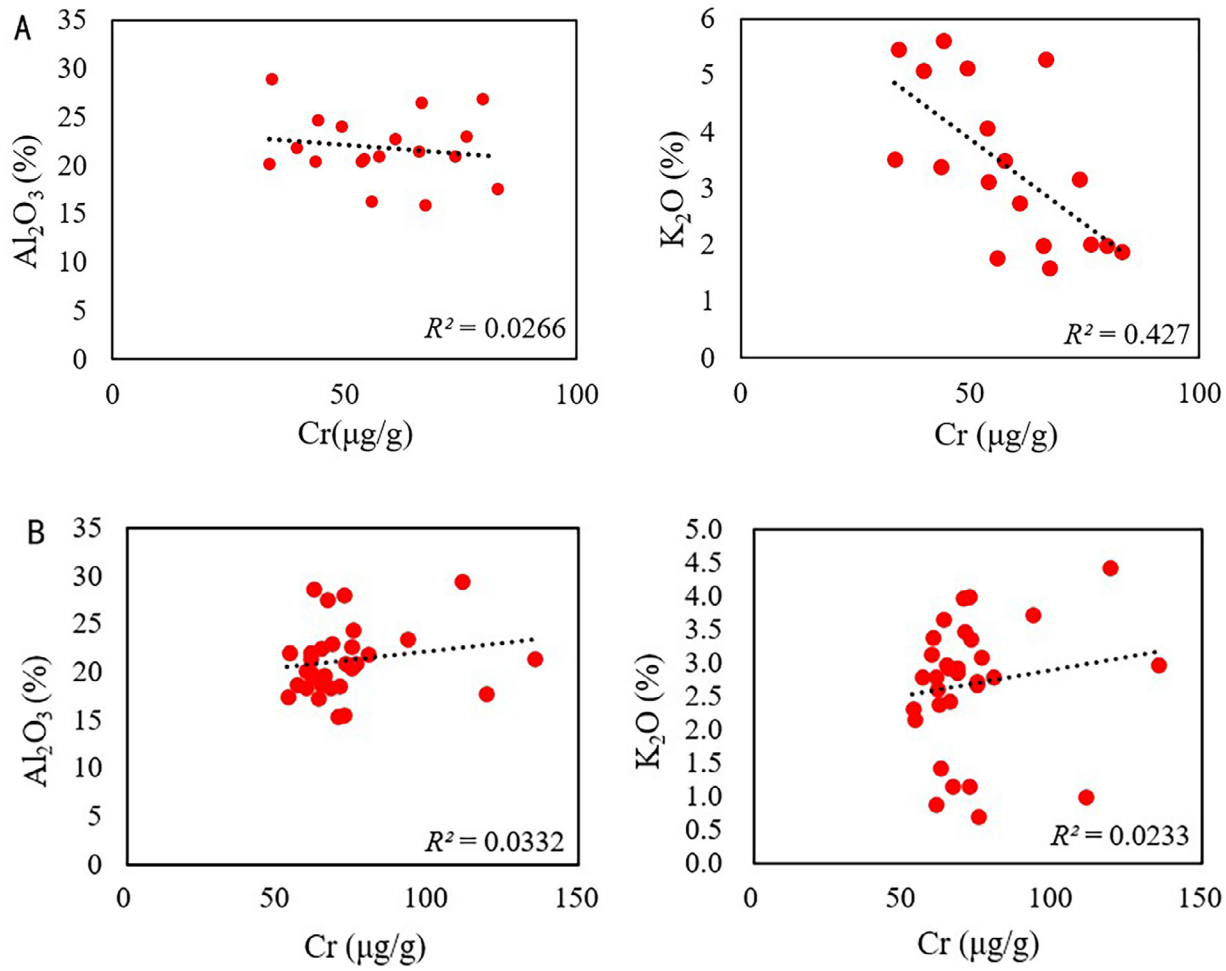


Figure 19. Correlation between Cr content, aluminium oxide (Al_2O_3), and potassium oxide (K_2O). (A) Taiyuan Formation coal-bearing shale. (B) Upper Paleozoic mudstone.

$$\delta Ce = \frac{Ce}{Ce^*} = \frac{Ce_N}{\sqrt{La_N \times \mathrm{Pr}_N}} \quad (2)$$

$$\delta La = \frac{La}{La^*} = \frac{La_N}{\sqrt{Ce_N \times \mathrm{Pr}_N}} \quad (3)$$

Among them, Eu_N, Sm_N, Gd_N, Ce_N, La_N, and Pr_N are the standardized values of chondrites of Eu, samarium, gadolinium, Ce, lanthanum (La), and praseodymium, respectively. Equations 1–3 calculate the abnormal Eu, Ce, La, and Y/Ho ratio in the Shiqianfeng Formation–Benxi Formation of the LX-5 well. The results are shown in Figure 21.

All samples exhibited negative Eu anomaly characteristics, which were notably different from the strong positive Eu anomaly characteristics of high-temperature hydrothermal fluids on the seabed. Therefore, the source of REE was not hydrothermal. Moreover, the light REE enrichment, Ce positive anomaly, lower Y/Ho ratio, and La positive anomaly in the samples were markedly different from the distribution characteristics of REE in seawater. Therefore, the source of REE was not from seawater or marine organisms.

4.6.3. Controls and enrichment mechanisms of chromium in coal-bearing strata

The enrichment and distribution of chromium (Cr) in the study area's coal-bearing strata are not attributable to a single geological event but a result from the complex interplay of syndepositional environmental conditions and subsequent tectonic-hydrothermal overprinting. The following points outline the distinct mechanisms driving Cr accumulation, highlighting the transition from primary sedimentary controls to secondary hydrothermal

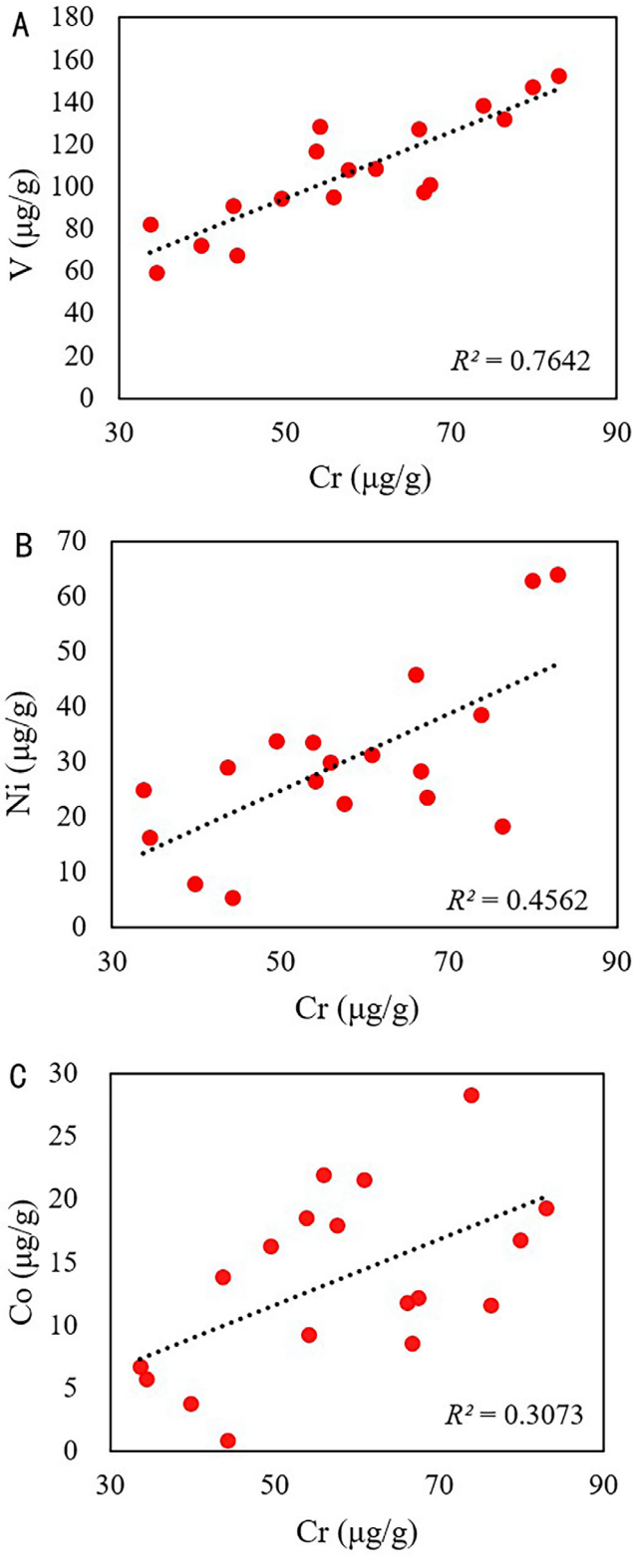


Figure 20. Correlation between chromium (Cr) and various elements in the lower coal-bearing shale of the Taiyuan Formation. (A) Cr and vanadium (V). (B) Cr and nickel (Ni). (C) Cr and cobalt (Co).

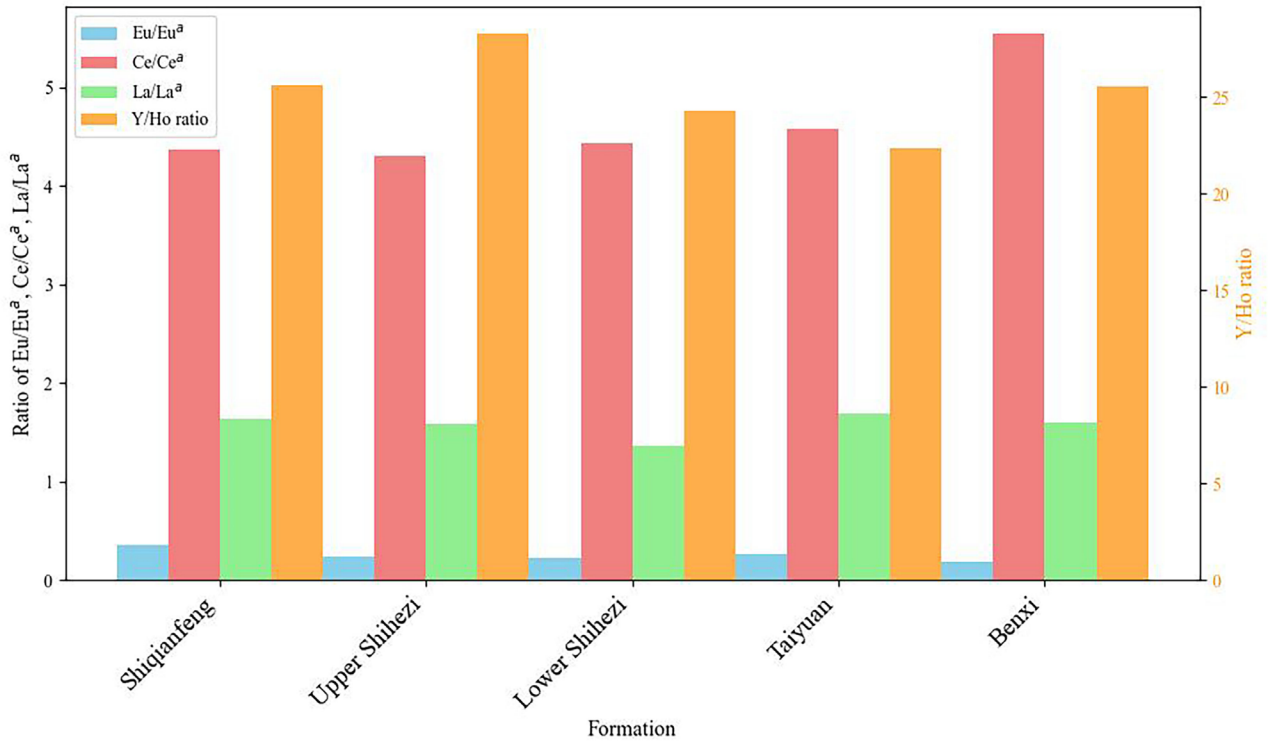


Figure 21. Europium (Eu), cerium (Ce), lanthanum (La) anomalies, and yttrium (Y)/holmium (Ho) ratio
Note: Eu^a: Theoretical Eu concentration calculated based on adjacent elements Sm and Gd; Ce^a: Theoretical Eu concentration calculated based on adjacent elements La and Pr; La^a: Theoretical Eu concentration calculated based on adjacent elements Ce and Pr.

modification and the challenges in quantifying their relative contributions.

(i) Cr element differences caused by volcanic hydrothermal activity:

The Cr element in the Paleozoic sandstone of this area showed significant stratigraphic differentiation across strata (Figure 22). The Lower Shihezi Formation exhibited extremely strong anomalies; the Taiyuan Formation had a high value and was mainly moderately enriched; and the Shanxi Formation samples generally showed regional, relatively uniform moderate enrichment. The Shiqianfeng Formation had significant fluctuations, and local high values may have multi-stage superposition or transformation characteristics. The stone box group was close to the background value (59.5–62.0 μg/g). Similarly, in the Upper Paleozoic sandstone samples, the Lower Shihezi Formation L5-18 was an outlier, with a Cr content (307.33 μg/g) close to 10 times the background value. Overall, high-value outliers showed significant locality and heterogeneity.

The differences in Figure 22 were mainly controlled by Yanshanian tectonic volcanic hydrothermal activity induced by the Zijinshan rock-mass uplift. The Taiyuan Formation, a reducing coal-bearing formation rich in organic matter and pyrite, experienced rapid Cr enrichment at fixed points. After hydrothermal fluids rose along the deep fault, precipitation and adsorption were triggered by a sudden drop in temperature and pressure and a strong reducing environment at the intersection of the fault, coal seam, and mudstone, leading to abnormal enrichment. The thick sandstone of the Lower Shihezi Formation had high pore permeability, making it an effective conduit for lateral hydrothermal fluid migration. A large fluid flux and water-rock reaction promoted widespread Cr precipitation in sandstone pores, cement, or sandstone-shale contact zones, forming a strong enrichment zone like L5-18. The Shanxi Formation may be on the periphery of the main channel, showing secondary diffusion and adsorption superposition of hydrothermal fluids during transport, resulting in a relatively stable background and moderate Cr enrichment. In contrast, the Shiqianfeng Formation lay in the uppermost layer and was less affected by deep hydrothermal fluids. Its Cr content reflected the initial background of terrestrial debris input and later surface fluid alteration, and local high values may be related to occasional fault communication.

In summary, the interlayer differences of Cr in the study area are dominated by volcanic hydrothermal events. High-value anomalies mainly develop near fault systems and are coupled with high-porosity, permeable sandstones or strongly reducing organic-rich layers. Moderate enrichment reflects the regional effect of hydrothermal diffusion superimposed on the original sedimentary background. This implies that when predicting the associated enrichment of critical metals in coal measures, priority should be given to favorable sections controlled by deep faults around the uplifted rock mass, sandstone channels of the Lower Shihezi Formation, and reducing coal-bearing traps of the Taiyuan Formation.

(ii) Cr element response and sedimentary environment: Figure 23 shows a planar distribution map of Cr element content in the lower coal-bearing shale of the Taiyuan Formation in the study area, with the red box area representing the 3D seismic study area. Based on the RMS amplitude attributes and sedimentary microfacies interpretations of the Shanxi and Taiyuan formations (Figure 7), the corresponding relationships among seismic attributes, sedimentary microfacies, and element-enrichment response were established.

The Cr content was relatively high in the northern study area, and the overall Cr level in the 3D study area was moderate to high. Based on sedimentary facies distribution, high-value Cr areas often correspond to low-energy muddy sedimentary zones. As a typical iron-clay element, Cr is easily enriched in fine-grained sediments through multiple complexation and adsorption processes. Under relatively reduced sedimentary-interface conditions, its migration loss is reduced, which is beneficial for preservation. Therefore, static or weak hydrodynamic environments, such as distributary bays, lagoons, and tidal flats, are conducive to the deposition and preservation of fine-grained materials, organic matter, and Cr enrichment in muddy sediments. In contrast, high-energy sandy microfacies are usually not conducive to Cr enrichment due to increased particle size and dilution.

In summary, Cr enrichment in the study area is jointly controlled by low-energy, fine-grained sedimentation and relative reduction preservation conditions, and its spatial distribution exhibits a strong coupling with muddy microfacies.

(iii) Relative contributions of syndepositional and

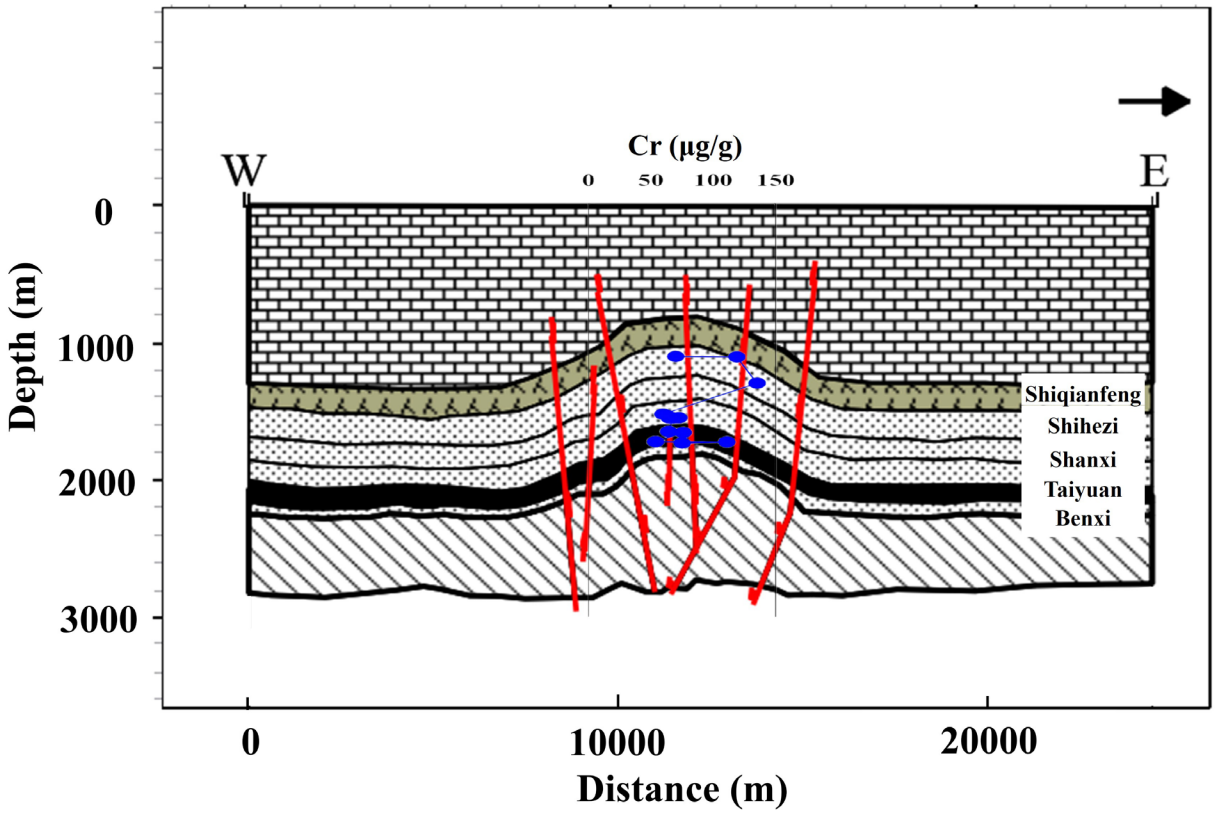


Figure 22. The variation of chromium (Cr) element content in Upper Paleozoic mudstone.

hydrothermal enrichment:

While this study delineates a multi-stage enrichment model for Cr, a quantitative assessment of the relative contributions from syndepositional versus post-depositional hydrothermal processes remains challenging. The anomalous Cr enrichment observed in the Lower Shihezi Formation (sample L5-18) and the localized high-value zones in the Taiyuan Formation are interpreted as resulting from synergistic effects between initial sedimentary concentration and subsequent hydrothermal remobilization. However, the overprinting of primary geochemical signatures by hydrothermal fluids, the potential mixing of multiple metal sources, and the absence of unique tracers exclusively tied to a single process currently preclude a precise quantitative partitioning. Future studies employing coupled isotopic systems (e.g., Cr, Sr, and neodymium), high-resolution micro-analytical techniques on mineral phases, and reactive transport modeling could help to disentangle these contributions. Nevertheless, the qualitative framework established here, which emphasizes the sequential roles of sedimentary reduction, fault-controlled fluid channeling, and groundwater-mediated redistribution, provides a robust foundation for identifying exploration targets where such multi-stage enrichment is most likely to occur.

4.6.4. Multi-factor comprehensive mineralization

Based on the systematic analysis, a "source transport accumulation" dynamic mineralization model was developed for key metals such as Cr in coal-bearing strata:

(i) Source stage

The key metals (such as Cr, Ga, and Zr) mainly originate from the weathering and erosion products of aluminum potassium granite and basic/ultrabasic rocks in the northern Yinshan ancient land. These sources, in the form of stable heavy minerals, such as chromite and clay minerals, are transported by rivers into sedimentary basins.

(ii) Same sedimentary enrichment stage

In the warm and humid freshwater tidal-delta barrier-island reduction environment of the Taiyuan Formation, metals are mainly adsorbed onto clay minerals or initially deposited onto heavy mineral particles. The strong reduction conditions, high organic matter content, and presence of sulfides promote the initial fixation of metals through sulfurization, organic complexation, and adsorption onto fine-grained sediments. At this stage, the chemical properties of pore water (early diagenetic groundwater) in sediments, such as oxygen deficiency and sulfur content, directly control the stability and organic complexation efficiency of metal sulfides. The geochemical gradient generated by salinity fluctuations caused by marine invasion further affects the distribution of metals between water and sediment. At this stage, a regional background enrichment pattern, constrained by stratigraphy, formed.

(iii) Postnatal transformation and secondary enrichment stage

The Yanshanian tectonic thermal event (related to the Zijinshan pluton) is the key to triggering secondary enrichment. This stage involves two interrelated fluid systems: one is magma hydrothermal fluid originating

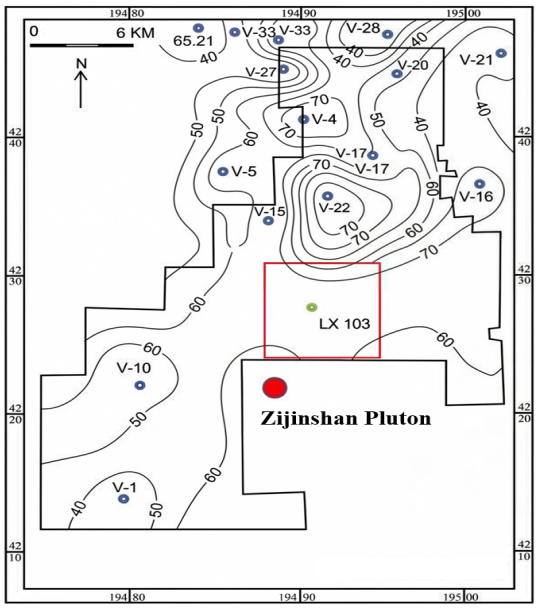


Figure 23. The plane distribution map of chromium content (μg/g) in coal measure shale of the Lower Taiyuan Formation

from the rock mass, upwelling along deep faults and fracture networks; The second is the groundwater in the basin that is supplied by the eastern edge of the basin and circulated under the joint control of sedimentary facies (high-permeability sandstone) and structurally-enhanced permeable zones (fault zones). The fault fissure system provides an advantageous transport pathway for both deep hydrothermal fluids and ancient groundwater. The mixing of two fluids, the formation of redox interfaces, and the long-distance transport of groundwater guided by structures collectively drive the activation and migration of fixed metals, and result in reprecipitation at favorable locations, such as fault intersections, high porosity and permeability sandstones, or reducing traps, ultimately leading to local high-grade enrichment.

5. Conclusion

Based on the integrated analysis of multi-source geophysical, geochemical, and geological data from the eastern margin of the Ordos Basin, this study elucidates the multi-stage enrichment mechanisms of critical metals within the coal-bearing strata.

The sedimentary environment of the Taiyuan Formation, characterized by a warm-humid, freshwater-influenced tidal delta-barrier island system, established the primary geochemical baseline. The resulting reducing and organic-rich conditions favored the initial sequestration of metals, including Zr, Cr, Ni, and Hf, through processes such as sulfidation and organo-complexation. Subsequent Yanshanian tectono-thermal events, associated with the Zijinshan pluton, were pivotal drivers of secondary enrichment. The magmatic activity generated fault and fracture networks that served as primary conduits for metal-bearing hydrothermal fluids, leading to localized, high-grade enrichment within high-porosity sand bodies and fault zones. Groundwater circulation played a critical and previously underappreciated role as a mobilizing agent. Recharged from the eastern basin margin, paleo-groundwater flow, regulated by sedimentary facies and fracture systems, facilitated the remobilization, redistribution, and reprecipitation of metals in response to hydrological and redox gradients. A focused study on Cr enrichment delineates a representative three-stage model: source weathering (terrigenous input), sedimentary reduction (initial fixation), and post-depositional tectonic-hydrothermal-groundwater activation (secondary enrichment). This model underscores the coupled influence of provenance, depositional setting, and post-depositional fluid activity.

The structure–sedimentation–groundwater coupled joint ore-controlling model established in this study deepens and enriches the previous conceptual framework regarding the control of minerals by single geological processes. It also clarifies the crucial bridging and core driving functions of ancient groundwater systems in this context. In contrast to previous studies that have predominantly focused on static reservoirs or isolated hydrothermal systems, this paper reveals the spatial framework of dominant groundwater transport pathways through high-precision wave impedance inversion and 3D attribute–structure coupling modeling. Moreover, by comprehensively leveraging geochemical indicators such as the Th/U ratio, it dynamically traces the oxidation-leaching activation ability and metal transport capacity. This model offers a more systematic and dynamic elucidation of the key metal mineralization mechanisms in coal-bearing strata and analogous basin environments. It also provides explicit predictive guidance for resource exploration in these areas.

Acknowledgments

None.

Funding

This study is supported by the Science Fund for Creative Research Groups of the National Natural Science Foundation of China (No. 42321002).

Conflict of interest

The authors declare no conflicts of interest.

Author contributions

Conceptualization: Yi Yang, Jingtao Zhao
Formal analysis: Yi Yang, Wanli Gao
Funding acquisition: Jingtao Zhao
Investigation: Suzhen Shi
Methodology: Yi Yang, Jingtao Zhao
Writing–original draft: Yi Yang
Writing–review & editing: Jingtao Zhao, Suzhen Shi

Availability of data

The data used in this study are restricted due to privacy and confidentiality agreements with the data providers. Data are available from the corresponding author upon reasonable request.

References

1. Ning SZ, Huang SQ, Liu K, *et al*. Comparison of genesis of abnormal enrichment of metals in coal between the northern and southern margins of Ordos Basin. *J China Coal Soc.* 2022;47(5):1795-1807.

doi: 10.13225/j.cnki.jccs.MJ22.0367

2. Cao B, Fu XH, Kang JQ, Tang P, Xu H. Enrichment Factors and Metallogenic Models of Critical Metals in Late Permian Coal Measures from Yunnan, Guizhou, and Guangxi Provinces. *Minerals*. 2024;14(2):206.

doi: 10.3390/min14020206

3. Cao DY, Qin GH, Zhang Y, *et al*. Classification and combination relationship of mineral resources in coal measures. *J China Coal Soc*. 2016;41(9):2150-2155.

doi: 10.13225/j.cnki.jccs.2016.0776

4. Zhao L, Dai SF, Nechaev VP, Nechaeva EV, Graham IT, French D. Enrichment origin of critical elements (Li and rare earth elements) and a Mo-U-Se-Re assemblage in Pennsylvanian anthracite from the Jincheng Coalfield, southeastern Qinshui Basin, northern China. *Ore Geol Rev.* 2019;115:103184.

doi: 10.1016/j.oregeorev.2019.103184

5. Zhao L, Wang XB, Dai SF. Lithium resources in coal-bearing strata: Occurrence, mineralization, and resource potential. *J China Coal Soc*. 2022;47(5):1750-1760.

doi: 10.13225/j.cnki.jccs.MJ22.0418

6. Ren DY, Zhao FH, Zhang JY, Xu D. A Preliminary study on genetic type of enrichment for hazardous minor and trace elements in coal. *Earth Sci Front.* 1999;6(z1):17-22.

doi: 10.3321/j.issn:1005-2321.1999.z1.003

7. Liu JJ, Dai SF, Song HJ, *et al*. Geological factors controlling variations in the mineralogical and elemental compositions of Late Permian coals from the Zhijin-Nayong Coalfield, western Guizhou, China. *Int J Coal Geol.* 2021;247:103855.

doi: 10.1016/j.coal.2021.103855

8. Dai SF, Wang PP, Ward CR, *et al*. Elemental and mineralogical anomalies in the coal-hosted Ge ore deposit of Lincang, Yunnan, southwestern China: Key role of N2–CO2-mixed hydrothermal solutions. *Int J Coal Geol*. 2015;152:19-46.

doi: 10.1016/j.coal.2014.11.006

9. Wei Q, Dai SF. Critical metals and hazardous elements in the coal-hosted germanium ore deposits of China: Occurrence characteristics and enrichment causes. *J China Coal Soc*. 2020;45(1):296-303.

doi: 10.13225/j.cnki.jccs.YG19.1633

10. Liu JJ, Han QC, Zhao SM, Jia R. The sources of abnormally enriched critical metals in the Late Permian coals of Western Guizhou Province. *J China Coal Soc*. 2022;47(5):1782-1794.

doi: 10.13225/j.cnki.jccs.MJ22.0178

11. Cao DY, Wei YC, Qin GH, *et al*. Tectonic control on enrichment and metallogenesis of strategic metal elements in coal measures. *Coal Geol Explor.* 2023;51(1):66-85.

doi: 10.12363/issn.1001-1986.22.09.0734

12. Zhang XL, He JX, Dong SH, Huang YP, Shi S, Wang W. Enrichment Characteristics and Genetic Analysis of the Strategic Metal Element Gallium in Coal-measure Shale, Lower Taiyuan Formation, Linxing Area. *Acta Sedimentol Sin.* 2022;40(6):1676-1690.

doi: 10.14027/j.issn.1000-0550.2022.110

13. Wu SG, Yu ZH, Zhang RQ, Han WG, Zou DB. Mesozoic–Cenozoic tectonic evolution of the Zhuanghai area, Bohai-Bay Basin, east China: the application of balanced cross-sections. *J Geophys Eng.* 2005;2(2):158-168.

doi: 10.1088/1742-2132/2/2/011

14. Sun QL, Wu SG, Lü FL, Yuan SQ. Polygonal faults and their implications for hydrocarbon reservoirs in the southern Qiongdongnan Basin, South China Sea. *J Asian Earth Sci.* 2010;39(5):470-479.

doi: 10.1016/j.jseaes.2010.04.002

15. Jamaludin SNF, Latiff AHA, Ghosh DP. Structural balancing vs horizon flattening on seismic data: Example from extensional tectonic setting. In: Gaol FL, Soewito B, editors. *IOP conference series: Earth and environmental science*. 2nd International Conference on Geological, Geographical, Aerospace and Earth Sciences 2014 (AeroEarth 2014); October 11–12, 2014; Bali, Indonesia. IOP Publishing; 2015;23(1):012003.

doi: 10.1088/1755-1315/23/1/012003

16. Budach I, Moeck I, Lüschen E, Wolfgramm M. Temporal evolution of fault systems in the Upper Jurassic of the Central German Molasse Basin: case study Unterhaching. *Int J Earth Sci.* 2018;107(2):635-653.

doi: 10.1007/s00531-017-1518-1

17. Quan H, Yu Z, Qiao Z, *et al*. Sedimentary and Early Diagenetic Responses to the Huaiyuan Movement During the Early–Middle Ordovician Transition in the Ordos Basin, North China. *Geosciences*. 2025;15(6):219.

doi: 10.3390/geosciences15060219

18. Qin GH, Deng LJ, Liu K, Xu H, Ma ZK, Cao DY. Characteristic of rare earth elements in coal in western margin of Ordos basin. *Coal Geol Explor.* 2016;44(6):8-14.

doi: 10.3969/j.issn.1001-1986.2016.06.002

19. Zhou XQ, Qin Y, Lu L. Advances on geological-geochemical research of coal-type uranium in China. *Coal Geol Explor*. 2019;47(4):45-53.

doi: 10.3969/j.issn.1001-1986.2019.04.008

20. Wang JQ, Deng JX, Xia H, Yan LL. Rock physics characteristics and their control factors of carbonate in different sedimentary microfacies of the Yingshan Formation, Gucheng Area, Tarim Basin. *J Geophys Eng.* 2023;20(6):1308-1321.

doi: 10.1093/jge/gxad087

21. Li XT, Lin CS. Delta front depositional system study based

on seismic attributes and well logging facies. *Appl Mech Mater.* 2012;170-173:1285-1289.

doi: 10.4028/www.scientific.net/AMM.170-173.1285

22. Wang Z, Xian BZ, Ma LC, Chao CZ, Pu Q, Liu JP. Mapping sediment-dispersal characteristics of Neogene deltas using seismic geomorphology, Liaodongdong area, Bohai Bay Basin, China. *Energy Sources Part A Recovery Util Environ Eff.* 2018;40(19):2265-2276.

doi: 10.1080/15567036.2018.1486477

23. Cao L, Chang S, Yao Y. Applying seismic sedimentology in predicting sedimentary microfacies and coalbed methane gas content. *J Nat Gas Sci Eng.* 2019;69:102944.

doi: 10.1016/j.jngse.2019.102944

24. Liu SM, Zhou L, Guan X, *et al*. Research on distribution characteristics of sedimentary microfacies of a system tract under a high resolution sequence framework: A case study of Qixia Formation in Gaomo block, central Sichuan. *Front Earth Sci.* 2023;11:1101242.

doi: 10.3389/feart.2023.1101242

25. Hower JC, Ruppert LF, Eble CF. Lanthanide, yttrium, and zirconium anomalies in the fire Clay coal bed, Eastern Kentucky. *Int J Coal Geol.* 1999;39(1-3):141–153.

doi: 10.1016/S0166-5162(98)00043-3

26. Mukhopadhyay PK, Goodarzi F, Crandlemire A.L, Gillis KS, MacNeil DJ, Smith WD. Comparison of coal composition and elemental distribution in selected seams of the Sydney and Stellarton Basins, Nova Scotia, Eastern Canada. *Int J Coal Geol*. 1998;37(1–2):113–141.

doi: 10.1016/S0166-5162(98)00020-2

27. Seredin VV, Finkelman RB. Metalliferous coals: a review of the main genetic and geochemical types. *Int J Coal Geol*. 2008;76(4):253–289.

doi: 10.1016/j.coal.2008.07.016

28. Dai SF, Ren DY, Li SS, Chou C. A Discovery of Extremely-enriched Boehmite from Coal in the Junger Coalfield, the Northeastern Ordos Basin. *Acta Geol. Sin*. 2006;80(02):294-300+315-316.

doi: 10.3321/j.issn:0001-5717.2006.02.015

29. Zou JH. Critical Elements Enrichment Mechanism of the Lopingian Coal-bearing Strata in the Eastern Sichuan Basin. PhD Thesis, China University of Mining and Technology (Beijing), Beijing; 2018.

30. Li Y, Wu P, Gao JX, *et al*. Multilayer coal-derived gas enrichment mechanism and whole gas-bearing system model: A case study on the Linxing block along the eastern margin of the Ordos Basin. *Nat Gas Ind*. 2022;42(6):52-64.

doi: 10.3787/j.issn.1000-0976.2022.06.005

31. Wu P, Gao LJ, Li Y, *et al*. An evaluation method for shale gas potential of marine-continent transitional facies with frequent interbedded lithology: A case study on the Lower Permian Shanxi Formation in Linxing block of the Ordos Basin. *Nat Gas Ind*. 2022;42(2):28-39.

doi: 10.3787/j.issn.1000-0976.2022.02.004

32. Du J, Zhu GH, Li Y, Wu P, Gao JX, Zhu YH. Exploration and development challenges and technological countermeasures for tight sandstone gas reservoirs in Ordos basin margin: A case study of Linxing-Shenfu gas field. *Nat Gas Ind*. 2022;42(1):114-124.

doi: 10.3787/j.issn.1000-0976.2022.01.011

33. Yue H, Guo P, Zhang T, *et al*. Integrated geophysical exploration of favorable potassium salt mineralization on the northeastern margin of Qaidam Basin, China. *J Geophys Eng.* 2025;22(3):889-900.

doi: 10.1093/jge/gxaf048

34. Li Y, Xu WK, Gao JX, *et al*. Mechanism of coal measure gas accumulation under integrated control of "source reservoir-transport system": A case study from east margin of Ordos Basin. *J China Coal Soc.* 2021;46(8):2440-2453.

doi: 10.13225/j.cnki.jccs.CB21.0765

35. Guo Q, Wang XY, Yin S, Wu ZH. Tectonic evolution and gas control analysis of the Upper Palaeozoic tight sandstone reservoirs in the Linxing area of the eastern Ordos Basin. *Geol. J.* 2021;56(3):1625-1637.

doi: 10.1002/gj.4007

36. Dai SF, Seredin VV, Ward CR, *et al*. Enrichment of U-Se-Mo-Re-v in coals preserved within marine carbonate successions: geochemical and mineralogical data from the Late Permian Guiding Coalfield, Guizhou.China. *Miner Depos.* 2015;50(2):159-186.

doi: 10.1007/s00126-014-0528-1

37. Fan YH, Qu HJ, Wang H, Yang XC. The application of trace elements analysis to identifying sedimentary media environment：A case study of Late Triassic strata in the middle part of western Ordos Basin. *Geol. China.* 2012;39(2):382-389.

doi: 10.3969/j.issn.1000-3657.2012.02.010

38. Jones B, Manning DAC. Comparison of geochemical indices used for the interpretation of palaeoredox conditions in ancient mudstones. *Chem Geol.* 1994;111(1-4):111-129.

doi: 10.1016/0009-2541(94)90085-x

39. Rimmer, SM. Geochemical paleoredox indicators in Devonian-Mississippian black shales, Central Appalachian Basin (USA). *Chem Geol*. 2004;206(3-4):373–391.

doi: 10.1016/j.chemgeo.2003.12.029

40. Shi J, Huang WH, Lv CH, Cui X. Geochemical characteristics and geological significance of the Upper Paleozoic mudstones from Linxing area in Ordos Basin. *Acta Pet Sin.*

2018;39(8):876-889.

doi: 10.7623/syxb201808004

41. Wu HC, He JX, Zhang XL, Ren ZQ, Zhou TT, Wang AK. Pore structure and its fractal features of the shale in Taiyuan Formation of Linxing area, Ordos Basin. *Xinjiang Pet Geol.* 2018;39(5):549-554.

doi: 10.7657/XJPG20180508

42. Tribovillard N, Algeo TJ, Lyons T, Riboulleau A. Trace metals as paleoredox and paleoproductivity proxies: an update. *Chem Geol*. 2006;232(1-2):12-32.

doi: 10.1016/j.chemgeo.2006.02.012

43. Dai SF, Ren DY, Chou CL, Finkelman RB, Seredin VV, Zhou YP. Geochemistry of trace elements in Chinese coals: A review of abundances, genetic types, impacts on human health, and industrial utilization. *Int J Coal Geol.* 2012;94:3-21.

doi: 10.1016/j.coal.2011.02.003

44. Finkelman RB, Bostick NH, Dulong FT, Senftle FE, Thorpe AN. Influence of an igneous intrusion on the inorganic geochemistry of a bituminous coal from Pitkin County, Colorado. *Int J Coal Geol*. 1998;36(3-4):223–241.

doi: 10.1016/S0166-5162(98)00005-6

45. Stewart AK, Massey M, Padgett PL, Rimmer SM, Hower JC. Influence of a basic intrusion on the vitrinite reflectance and chemistry of the Springfield (No. 5) coal, Harrisburg, Illinois. *Int J Coal Geol*. 2005;63(1-2):58–67.

doi: 10.1016/j.coal.2005.02.005

46. Sun R, Liu G, Zheng L, Chou CL. Geochemistry of trace elements in coals from the Zhuji Mine, Huainan Coalfield, Anhui, China. *Int J Coal Geol*. 2010;81(2):81–96.

doi: 10.1016/j.coal.2009.12.001

47. Russell BH. *Introduction to Seismic Inversion Methods*. Tulsa, OK, USA: Society of Exploration Geophysicists (SEG). 1988.

48. Yilmaz, Ö. *Seismic Data Analysis: Processing, Inversion, and Interpretation of Seismic Data*. Tulsa, OK, USA: Society of Exploration Geophysicists (SEG). 2001.

49. Azizzadeh Mehmost Olya B, Mohebian R, Moradzadeh A. A new approach for seismic inversion with GAN algorithm. *J Seism Explor.* 2024,33(3):01–36.

50. Zhang Y, Singh S, Thanoon D, Thanoon D, Devarakota P, Jin L, Tsvankin I. Physics-guided unsupervised deep-learning seismic inversion with uncertainty quantification. *J Seism Explor*. 2023;32(3):257–270.

51. Wang P, Xu HQ, Peng Z, Wang ZF, Yang MQ. Application of data augmentation based on generative adversarial network in impedance inversion. *J Seism Explor*. 2023;32(2):155–168.

52. Cai YD, Gao GS, Liu DM, Qiu F. Geological conditions for coal measure gas enrichment and accumulation models in Linxingzhong Block along the eastern margin of the Ordos Basin. *Nat Gas Ind.* 2022;42(11):25-36.

doi: 10.3787/j.issn.1000-0976.2022.11.003